Received: 13 August 2023 | Revised: 23 November 2023 | Accepted: 27 November 2023

DOI: 10.1002/hyp.15047

RESEARCH ARTICLE

WILEY

Assessing the sensitivity of modelled water partitioning to global precipitation datasets in a data-scarce dryland region

E. A. Quichimbo[1] | M. B. Singer[1,2,3] | K. Michaelides[3,4,5] | R. Rosolem[5,6] | D. A. MacLeod[1] | D.T. Asfaw[4] | M. O. Cuthbert[1,2,7]

[1]School of Earth and Environmental Sciences, Cardiff University, Cardiff, UK

[2]Water Research Institute, Cardiff University, Cardiff, UK

[3]Earth Research Institute, University of California Santa Barbara, Santa Barbara, California, USA

[4]School of Geographical Sciences, University of Bristol, Bristol, UK

[5]Cabot Institute for the Environment, University of Bristol, Bristol, UK

[6]Department of Civil Engineering, University of Bristol, Bristol, UK

[7]School of Civil and Environmental Engineering, The University of New South Wales, Kensington, New South Wales, Australia

Correspondence
E. A. Quichimbo, School of Earth and Environmental Sciences, Cardiff University, Cardiff, UK.
Email: quichimbomiguitamaea@cardiff.ac.uk

Funding information
European Union's Horizon 2020, Grant/Award Number: 869550; Global Challenges Research Fund; International Atomic Energy Agency of the United Nations; Natural Environment Research Council, Grant/Award Number: NE/T005645/1; Royal Society, Grant/Award Number: CHL\R1\180485; U.S. Department of Defenses Strategic Environmental Research and Development Program, Grant/Award Number: RC18-1006; U.S. National Science Foundation, Grant/Award Numbers: BCS-1660490, EAR-1700555; UK Natural Environment Research Council, Grant/Award Number: NE/P017819/1

Abstract

Precipitation is the primary driver of hydrological models, and its spatial and temporal variability have a great impact on water partitioning. However, in data-sparse regions, uncertainty in precipitation estimates is high and the sensitivity of water partitioning to this uncertainty is unknown. This is a particular challenge in drylands (semi-arid and arid regions) where the water balance is highly sensitive to rainfall, yet there is commonly a lack of in situ rain gauge data. To understand the impact of precipitation uncertainty on the water balance in drylands, here we have performed simulations with a process-based hydrological model developed to characterize the water balance in arid and semi-arid regions (DRYP: DRYland water Partitioning model). We performed a series of numerical analyses in the Upper Ewaso Ng'iro basin, Kenya driven by three gridded precipitation datasets with different spatio-temporal resolutions (IMERG, MSWEP, and ERA5), evaluating simulations against streamflow observations and remotely sensed data products of soil moisture, actual evapotranspiration, and total water storage. We found that despite the great differences in the spatial distribution of rainfall across a climatic gradient within the basin, DRYP shows good performance for representing streamflow (KGE >0.6), soil moisture, actual evapotranspiration, and total water storage (r >0.5). However, the choice of precipitation datasets greatly influences surface (infiltration, runoff, and transmission losses) and subsurface fluxes (groundwater recharge and discharge) across different climatic zones of the Ewaso Ng'iro basin. Within humid areas, evapotranspiration does not show sensitivity to the choice of precipitation dataset, however, in dry lowland areas it becomes more sensitive to precipitation rates as water-limited conditions develop.

The analysis shows that the highest rates of precipitation produce high rates of diffuse recharge in Ewaso uplands and also propagate into runoff, transmission losses and, ultimately focused recharge, with the latter acting as the main mechanism of groundwater recharge in low dry areas. The results from this modelling exercise suggest that care must be taken in selecting forcing precipitation data to drive hydrological modelling efforts, especially in basins that span a climatic gradient. These results also suggest that more effort is required to reduce uncertainty between different precipitation datasets, which will in turn result in more consistent quantification of the water balance.

KEYWORDS
dryland, ephemeral streams, groundwater, recharge, transmission losses, water partitioning

1 | INTRODUCTION

Precipitation is a key driver of the terrestrial water balance and is the primary input to hydrological models that seek to quantify the availability of water resources. Precipitation is generally measured at points by rain gauges, but the limited spatial distribution of gauges in most places precludes their use for large-scale hydrological modelling (Daly et al., 1994; Groisman & Legates, 1994; Ly et al., 2013; McMillan et al., 2012; Pollock et al., 2018; Thornton et al., 1997). In dryland regions, this problem is exacerbated by the high spatial and temporal variability of precipitation (Goodrich et al., 1995; Huang et al., 2017; Pilgrim et al., 1988; Wheater et al., 2007) and the sparseness of data collection networks (Pilgrim et al., 1988; Wheater et al., 2007). Reanalysis and remotely sensed gridded precipitation products have potential to overcome the limited spatial distribution of point observations of precipitation, and some have high temporal resolution required to characterize individual rainstorms. However, such gridded rainfall products contain inherent uncertainties that are pronounced in dryland environments and in mountainous topography (Ayugi et al., 2019; Coz & van de Giesen, 2020; Dezfuli et al., 2017; Dinku et al., 2018; Guilloteau et al., 2016; Henn et al., 2018; Huang et al., 2017; Lettenmaier et al., 2015; Lundquist et al., 2015; Macharia et al., 2020; Sylla et al., 2013; Westrick et al., 1999). These uncertainties in precipitation propagate into unknown impacts on water partitioning and consequently limit the usefulness of gridded rainfall products to force hydrological models in these regions (Fu et al., 2011; Huang et al., 2019; Ly et al., 2013; Obled et al., 1994; Schreiner-McGraw & Ajami, 2020).

The ability to model the partitioning of rainfall into water stores and fluxes in dryland environments is of key importance for assessing the availability of water resources in such water-limited ecosystems. In these regions, precipitation is typically delivered in short-lived but high intensity events, with most of the water reaching the land surface lost back to the atmosphere via evapotranspiration (Goodrich et al., 1995; Pilgrim et al., 1988; Wheater et al., 2008). In drylands, the combination of high rainfall intensities and low infiltration rates partitions precipitation into some combination of overland flow and infiltration, depending on storm intensity and duration for a given land surface condition (Aryal et al., 2020; Goodrich et al., 1997; Scoging & Thornes, 1979; Zhu et al., 2018). Runoff events tend to be short-lived, yet the flow may coalesce to support the development of ephemeral streams. The loss of water through the typically porous streambed of these ephemeral streams, known as transmission losses, potentially generates focused recharge (Quichimbo et al., 2020), which is considered to be the main process of groundwater recharge in dryland environments (Abdulrazzak, 1995; Goodrich et al., 1995; Goodrich et al., 2013; Goodrich et al., 2018; Schreiner-McGraw et al., 2019; Shanafield & Cook, 2014). Since these key dryland hydrological processes are controlled by the high variability in rainfall intensity and duration, it is therefore important to understand how the spatial and temporal variation of the choice of forcing precipitation dataset impacts water partitioning. This in turn will enhance the characterization and quantification of key hydrological processes that represent the water balance of these dry environments.

A variety of studies have focused on the accuracy and the spatio-temporal agreement between gridded rainfall datasets (e.g., (Alexander et al., 2020; Ayugi et al., 2019; Dezfuli et al., 2017; Dinku et al., 2018; Macharia et al., 2020; Maggioni et al., 2016; Massari et al., 2017; Tang et al., 2020)). Studies evaluating the impact of rainfall variability on hydrological response using process-based hydrological models are limited (e.g., (Beck et al., 2017; Satgé et al., 2021; Schreiner-McGraw & Ajami, 2020; Stisen & Sandholt, 2010)). Approaches instead typically rely on models that do not consider key dryland hydrological processes, such as transmission losses and focused recharge (Beck et al., 2017; Bitew et al., 2012; Dembélé et al., 2020; Li et al., 2012; Su et al., 2008; Tang et al., 2016). Additionally, most of these studies typically only use streamflow for model calibration, and do not evaluate the uncertainty of model parameterisation on the broader water partitioning (Maggioni et al., 2016).

Here, we use the distributed, integrated, hydrological model DRYP (Quichimbo, 2021) to quantify the water partitioning at the Upper Ewaso Ng'iro basin in Kenya because it is a model designed to represent the hydrological processes that are explicitly relevant in dryland environments such as spatio-temporally varying and high

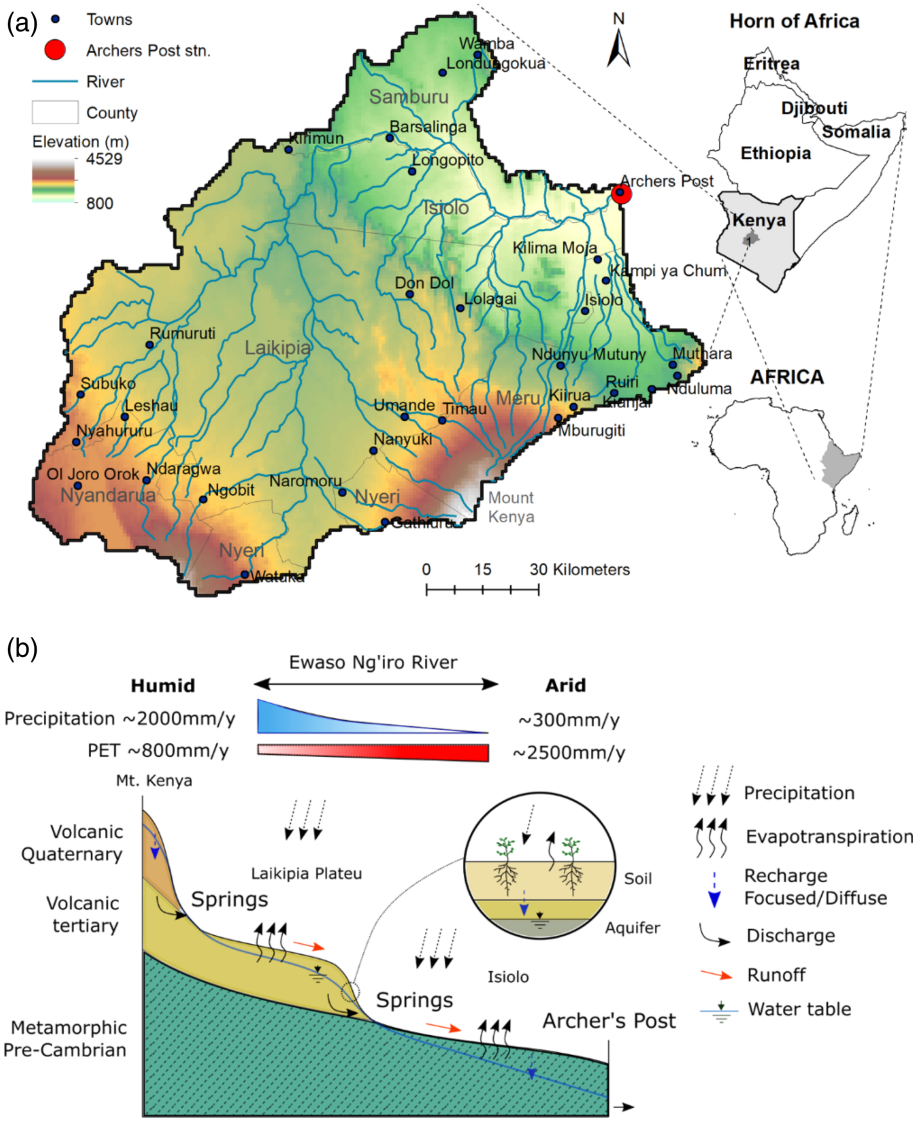

FIGURE 1 (a) Geographical location of the Upper Ewaso Ng'iro basin, and (b) Conceptual schematic detailing key climatological, hydrological, and hydrogeological factors controlling the water partitioning of the Upper Ewaso Ng'iro basin. Arrows indicate main fluxes.

intensity rainfall, high evaporative losses, transmission losses, focused recharge, and the development of ephemeral streams. We applied three widely used gridded precipitation datasets, available at high spatial and temporal resolutions (sub-daily and 0.1°) to force the DRYP model, and we evaluate model performance using a variety of remotely sensed data and streamflow observations. Ultimately, we perform a series of numerical experiments to test how the spatial variability of precipitation affects the uncertainty in the components of the water balance.

2 | DATA AND METHODS

2.1 | Study area

The upper Ewaso Ng'iro basin is located northwest of Mount Kenya (Figure 1a) with an area of ~15 200 km^2 and elevations ranging from ~800 m in its lower northeastern part (Archer's Post) to ~4700 m at the top of Mt. Kenya in the southern headwaters (Figure 1a). The basin exhibits distinct hydrological regimes depending on elevation, latitude, and the location of the Intertropical Convergence Zone over the year (Figure 1b). Unimodal (one season) rainfall characteristics are observed in the western part of the basin, whereas two well-defined rainy seasons characterize the climate of Mount Kenya and the lower parts of the basin (Ngigi et al., 2008). In the bimodal rainfall locations, the 'long rains' generally occur between March–May and the 'short rains' occur in October–December (Ngigi et al., 2008). Precipitation exhibits high interannual variability and is also dependent on topography with high average annual precipitation (~1700 mm) at high elevations (>3300 m), lower precipitation (~800 mm) at elevations between 2000 and 1700 m on the Laikipia plateau, and much low values of precipitation (~350 mm) in lower elevations around the catchment outlet (Archer's Post) (Gichuki, 2002; Liniger et al., 2005; Muriithi, 2016; Mutiga et al., 2010; Notter et al., 2007). Potential evapotranspiration also has high spatial variation with mean annual values of ~500 mm at high elevations to ~1700 mm at lower ones (Ngigi et al., 2007). The basin is mostly covered by woody vegetation, shrublands, and grasses (Franz et al., 2010; Franz et al., 2012;

Gichuki, 2004; Mati et al., 2006; Muriithi, 2016; Mutiga et al., 2010). Geologically, the upper part of the basin is underlain by Quaternary and Tertiary volcanic material, whereas outcrops of metamorphic rocks from the Basement system dominate the geology of the lower areas (Figure 1b) (Muriithi, 2016).

We expect the complex topographic, geological and climatological characteristics to strongly influence the hydrological processes and water balance of the basin (Figure 1b). For example, the strong gradients in precipitation and potential evapotranspiration may contribute to the development of contrasting dominance of certain hydrological fluxes at higher (e.g., more diffuse recharge and baseflow) versus lower elevations (e.g., more focused recharge).

2.2 | Forcing datasets

2.2.1 | Precipitation and potential evapotranspiration

Owing to their high temporal and spatial resolution, the following global datasets of precipitation were used as forcing data for water partitioning evaluation, all of which are available at 0.1° grid resolution (~9 km at the equator) (i) the 3-h Multi-Source Weighted-Ensemble Precipitation (MSWEP) V2.8 Global, (ii) the 30-min resolution Integrated Multi-satellitE Retrievals for Global Precipitation Measurement (IMERG) V06A, and (iii) the 1-h ERA5 – reanalysis precipitation dataset (Table 1). The high temporal and spatial resolution of these precipitation datasets is commensurate with the timescales (sub-daily) of the main hydrological processes within dryland basins (Quichimbo, 2016) where rainfall tends to occur in high intensity, short duration (sub-daily and even sub-hourly) events. To compare their influence, each dataset was aggregated to a consistent 3 h for simulations in the Ewaso Ng'iro basin, corresponding with the MSWEP resolution. All these datasets have shown good performance in representing the climatological conditions as well as the hydrology when used as forcing data in dryland environments (Beck et al., 2017), although, convective precipitation events in dryland regions are challenging to capture within these gridded datasets (Cecil et al., 2014).

Owing to its sufficiently high spatio-temporal, the global dataset of hourly Potential EvapoTranspiration (hPET) (Singer et al., 2021) was used as a forcing variable for driving plant and soil evaporation water demands from the atmosphere. hPET is a product based on ERA5-Land reanalysis dataset with a spatial resolution of 0.1° to match the rainfall datasets and estimates potential evapotranspiration using the Penman-Monteith approach.

2.3 | Parsimonious dryland water partitioning hydrological model: DRYP

DRYP is an integrated, parsimonious, process-based, distributed hydrological model developed to represent key hydrological processes in dryland regions (Quichimbo et al., 2021). The model includes three

TABLE 1 Forcing datasets used for model simulations.

Data set	Data type	Resol.	Freq.	Coverage	Period	Data source/model	Reference
Precipitation datasets							
MSWEP v2.8 (MSWEP)[a]	Satellite-based	0.1°	3 h	Global	1979–present	CPC, GPCC, CMORPH, GSMaP-MVK, TMPA, ERA-Interim, JRA-55	Beck et al. (2019)
IMERG Final (IMERG)[b]	Satellite-based	0.1°	30 min	60° S–60° N	2001–present	GMI, AMSR-2, SSMIS, Madaras, MHS, Advanced Technology Microwave Sounder	Huffman et al. (2015)
ERA5 (ERA)[c]	Reanalysis	0.1°	1 h	Global	1979–present	European Centre for Medium-Range Weather Forecasts (ECMWF)	Hersbach et al. (2020)
Potential Evapotranspiration dataset							
hPET[d]	Derived from reanalysis	0.1°	1 h	Global	1981–present	Penman-Monteith, ERA5-Land	Singer et al. (2021)

[a]MSWEP: https://www.gloh2o.org/mswep/ (last accessed: 20/02/2023).
[b]IMERG: https://gpm1.gesdisc.eosdis.nasa.gov/ (last accessed: 20/02/2023).
[c]ERA5: https://cds.climate.copernicus.eu/cdsapp#!/dataset/reanalysis-era5-single-levels?tab=form (last accessed: 20/02/2023).
[d]hPET: https://doi.org/10.5523/bris.qb8ujazzda0s2aykkv0oq0ctp (last accessed: 01/02/2023).

main components: (i) a surface component to represent the infiltration and runoff as well as transmission losses along streams, (ii) a subsurface component that represents the vadose zone where plant evapotranspiration and percolation occurs, and (iii) a groundwater component to represent the flow under saturated conditions. A simplified version of the water balance equation is shown below, and a detailed description of the model can be found in Quichimbo et al. (2021).

$$P = OF + I \tag{1a}$$

$$\Delta S_{RO} = OF + BF - TL - Q \tag{1b}$$

$$\Delta S_{UZ/RUZ} = I + TL - AET - R \tag{1c}$$

$$\Delta S_{SZ} = R - AET_{GW} - BF - BC \tag{1d}$$

where: P is precipitation [L T^{-1}], I is infiltration [L T^{-1}], OF is overland flow [L T^{-1}], TL is transmission losses [L T^{-1}], AET is actual evapotranspiration [L T^{-1}], AET_{GW} is capillary flux [L T^{-1}], R is diffuse and focused recharge of hillslope and riparian zone, respectively, [L T^{-1}], BF is groundwater discharge [L T^{-1}], Q is channel streamflow [L T^{-1}], BC is any source of water getting in/out of the saturated zone [L T^{-1}], Δ represent change, and $S_{UZ/RUZ}$, S_{RO}, and S_{SZ}, represent the unsaturated/riparian zone, channel and groundwater storage [L], respectively.

2.3.1 | Model settings and parameterisation

For the Ewaso Ng'iro basin, the spatial and temporal resolution of the model was set on a 1 × 1 km grid (201 × 174 cells) and 3-h time step, respectively. This resolution was chosen in order to adequately represent the spatial and temporal variability of key hydrological fluxes such as streamflow and transmission losses along channels (Quichimbo, 2021) as well as the short-lived rainfall in drylands. The 3-h time step is also considered reasonable for two main reasons: (i) it is a trade-off between the computational time and process description representation (Quichimbo, 2021), and (ii) it matches the temporal resolution of available precipitation datasets. The forcing datasets, which are at a spatial resolution of 0.1°, were spatially interpolated to the model spatial resolution of 1 km, using linear interpolation due to its low computational demand.

For the unsaturated zone, the Philips infiltration equation, implemented using an explicit numerical approach, was applied since it showed good performance for modelling water partitioning in the semi-arid Walnut Gulch Experimental Watershed (Quichimbo, 2021). For the groundwater component, a variable transmissivity approach was specified for groundwater flow in the saturated model component, which allows the representation of the reduction of transmissivity with depth due to less weathered conditions (Bianchi et al., 2020; Bonsor et al., 2014; Fan et al., 2013). A detailed description of the approach and its numerical implementation is described in Quichimbo, 2021.

Table 2 provides a summary of datasets used for the parameterization of each of the model components. A full description of the dataset as well as the parameters derived from the dataset are provided in the supplemental material (Section S2.2).

2.3.2 | Boundary and initial conditions

It is assumed that the groundwater system in the Ewaso Ng'iro basin is shallow, therefore, topographical conditions greatly influence surface and groundwater processes. Hence, no-flow boundary conditions for the groundwater domain were specified along the boundaries of the basin. To avoid the artificial accumulation of water in lower parts of the basin, a constant head boundary was specified at the lowest end of the model domain where there is an outcrop of the Basement aquifer system (Figure S1f). The values were specified to be equivalent to a depth to the water table of 20 m below the stream based on observations reported nearby (WRAP, 1987).

A dynamic cyclic equilibrium approach was used to assign the initial conditions of the unsaturated and saturated zone of the model. Dynamic cyclic conditions were reached after running the model repeatedly for the period 1 January 2001–31 December 2010. A more detailed description of the approach is presented in the Supplemental Material S2.2.

2.3.3 | Evaluation datasets

In situ measurements of soil moisture, evapotranspiration, or water table depth at appropriate temporal scales (daily/monthly) are not available for the study area. Therefore, the following remotely sensed products were used to evaluate the spatial and temporal variation of model outputs: actual evapotranspiration from Moderate Resolution Imaging Spectroradiometer (MODIS – MOD16ET); soil moisture from the European Space Agency Climate Change Initiative (ESA-CCI), and total water storage from the Gravity Recovery and Climate Experiment (GRACE) (Table 3).

Remote sensing products have shown good performance in representing seasonality in evapotranspiration (ET), soil moisture, and total water storage over different regions around the world (Blatchford et al., 2020; Cleugh et al., 2007; Mayes et al., 2020; Mutiga et al., 2010). However, absolute values for these remote sensing products used over similar semi-arid dominated environment have shown great uncertainty. For example: MOD16 ET has shown good skill in representing monthly fluctuations although it has shown low values of ET in dry regions, which is mainly attributed to land cover heterogeneity (Aguilar et al., 2018; Blatchford et al., 2020; Jahangir & Arast, 2020; Kiptala et al., 2013; Miralles et al., 2016; Trambauer et al., 2014; Velpuri et al., 2013; Weerasinghe et al., 2020). For soil moisture, ESA-CCI is only representative of the soil depth between 2 and 5 cm (Brocca et al., 2017); therefore, it cannot be directly compared to the single depth integrated DRYP soil store. Finally, for total water storage, the uncertainty of GRACE estimates of total water

TABLE 2 Datasets used for model parameterisation, details about the calibration factor k is provided in section 2.4.

Parameter	Description	Dataset/default values	Calibration (k-factor)*
Surface and Overland flow			
z	Surface elevation	SRTM 1 Arc-Second Global dataset	Not applicable
z_{riv}	River bottom elevation	30th percentile of SRTM 1	Not applicable
L_{ch}	Channel length	Derived from SRTM 1	Not applicable
k_T	Recession time for channel streamflow	0.083 h^{-1}*	0.15–0.55
W	Channel width	10 m*	Not calibrated
K_{ch}	Channel saturated hydraulic conductivity	(Dai et al., 2019)	0.2–1.0
Unsaturated zone			
K_{sat}	Saturated hydraulic conductivity	(Dai et al., 2019)	0.1–0.5
ψ	Suction head	(Dai et al., 2019)	Not calibrated
λ	Soil pore size distribution	(Dai et al., 2019)	Not calibrated
θ_{sat}	Saturated water content	(Dai et al., 2019)	Not calibrated
θ_{wp}	Water content at wilting point	Derived from (Dai et al., 2019)	Not calibrated
θ_{fc}	Water content at field capacity	Derived from (Dai et al., 2019)	Not calibrated
D	Rooting depth	(Leenaars et al., 2018)	0.6–2.0
Saturated Zone			
S_y	Specific yield	GLHYMPS (Gleeson et al., 2014)	0.01–0.2
K_{aq}	Saturated hydraulic conductivity	GLHYMPS (Gleeson et al., 2014)	5.0–35.0
f_D	Effective aquifer depth	(Pelletier et al., 2016)	Not calibrated

*Range of factor values specified during model calibration (Section 2.4).

TABLE 3 Datasets used for model evaluation (a detailed description is provided in the Supplemental section S2.2).

Name	Dataset	Res.	Freq.	Coverage	Period	Data source	Reference
MOD16 ET	Evapotranspiration	500 m (∼0.0045°)	8-day	global	2000-present	MODIS (land cover, albedo, leaf area index, and Enhanced Vegetation Index)	Mu et al. (2007); Running et al. (2017)
ESA-CCI	Soil moisture	0.25°	1-day	global	2000-present	combined solution: passive (radiometer) and active (scatterometer/radar) sensors	Dorigo et al. (2017); Liu et al. (2011); Preimesberger et al. (2021)
GRACE	Total water storage (TWS)	1°	1-month	Global	2003-present	Mascons solutions (JPL and CSR)	(Rowlands et al., 2005; Save et al., 2016; Watkins et al., 2015)

Note: MODIS: Moderate Resolution Imaging Spectroradiometer, https://lpdaac.usgs.gov/products/mod16a2v006/ (last accessed: 10/02/2022); ESA: European Space Agency, https://www.esa-soilmoisture-cci.org/ (last accessed: 15/02/2023); GRACE: Gravity Recovery And Climate Experiment, http://grace.jpl.nasa.gov (last accessed: 20/02/2023).

storage changes (TWSC) depends on factors such as the post-processing approach, region, and basin size. For basins smaller than 200 000 km^2, the uncertainty increases considerably due to leakage, therefore, the only GRACE mascons solutions are typically used (Landerer & Swenson, 2012; Longuevergne et al., 2010; Scanlon et al., 2012), an approach we follow here for evaluation of DRYP. Here we performed a correlation analysis between monthly average values of DRYP outputs to monthly averages of remotely sensed products, and we present the results in terms of *p*-values and correlation, *r*.

Finally, in addition to remote sensing datasets, streamflow observations, Q, available at the catchment outlet (Archers' Post station) (Figure 1a) were used for the model performance evaluation. Streamflow measurements were available for the period between 01 January 1960 and 12 October 2012. However, due to data gaps encountered in the period before 01 January 2000, only the period after that date was used for model evaluation, which also matches the available period of the IMERG forcing precipitation dataset. Considering the high variability of flow in dryland ephemeral streams, it is advisable to

use the longest available dataset for streamflow for model evaluation (Zoccatelli et al., 2020),

2.4 | Model calibration, sensitivity and uncertainty analysis

Model calibration was carried out in two stages. First, an initial trial-and-error calibration of the model was performed to explore the parameter sensitivities and to reduce the a priori parameter ranges used in the second step. The calibration was performed by applying spatially constant multiplicative factors (k), kK_{sat}, kD_{root}, kK_{ch}, kT, kK_{aq}, and kSy to model parameters K_{sat}, D_{root}, K_{ch}, T, K_{aq}, S_y (Table 1), respectively, which represent the dominant controls on the storage and water partitioning of the surface and subsurface components. The channel width, W, assumed to be constant over the model domain, was not evaluated because it is combined proportionally with hydraulic conductivity in the model equations (Quichimbo et al., 2021), and thus its sensitivity to change is represented by the parameter kK_{ch}. The initial trial-and-error calibration enabled a set of parameter ranges to be defined for a subsequent stage of model evaluation (Table 1). The second stage included a sensitivity analysis of model parameters through a Monte Carlo type analysis. The number of simulations used for this analysis was limited to only 500 realizations due to the long simulation times required for analysis. Each set of parameters were generated by using a uniform distribution.

To evaluate the performance of each set of parameters in representing streamflow at the catchment outlet (Archers' Post), we used a combination of two 'goodness of fit' indices: Kling-Gupta Efficiency (KGE) (Gupta et al., 2009) and per cent bias (PBIAS):

$$KGE = 1 - \sqrt{(r-1)^2 + (\alpha-1)^2 + (\beta-1)^2} \tag{2a}$$

$$\alpha = \frac{\sigma_S}{\sigma_O} \tag{2b}$$

$$\beta = \frac{\mu_S - \mu_O}{\sigma_O} \tag{2c}$$

$$PBIAS(\%) = 100 \cdot \beta \tag{3}$$

where: O represents the observation, S represent the simulations, r is the correlation coefficient, β is the bias, μ is the mean and σ is the standard deviation.

The KGE was used based on its ability to assess the temporal variability, bias and correlation between observed and simulated data over a time series, reducing the influence of peak values on the evaluation (Gupta et al., 2009; Krause et al., 2005). This is important to assess the contribution of low flows (baseflow) from the upstream areas in the study site. The KGE index already includes the bias term (β), however, as one of the goals here was to evaluate the water partitioning, the bias between observation and simulation was also explicitly evaluated using the PBIAS index.

To evaluate the sensitivity of model outputs to the parameters set, we specified a threshold for KGE and PBIAS. Thus, models run with a particular parameter sets which did not meet the threshold values for either KGE or PBIAS were rejected, whereas the models with values above that threshold where specified as behavioural. Threshold values for KGE and PBIAS were specified as 0.5% and ± 20%, respectively, given the high uncertainty of precipitation datasets. It is important to note that values of KGE ~ -0.41 indicate that simulations are not better than the mean value of the sample (Knoben et al., 2019).

Finally, in addition to the evaluation of streamflow, the selection of behavioural models was complemented with a correlation analysis between the available remote sense datasets (ESA-CCI, MOD16-ET, and GRACE) and their corresponding simulated values (soil moisture, actual evapotranspiration, and total water storage). Models were selected as valid when the correlation was >0.5. Given the uncertainty of remote sensing data, this threshold is considered to be acceptable, as it indicates a relationship between two variables.

2.5 | Assessing the sensitivity of water partitioning to precipitation datasets

To evaluate the sensitivity of water balance components to precipitation forcing, the distributions of mean hydrological fluxes from each behavioural model for each precipitation dataset were compared. The impact of precipitation on water partitioning was also evaluated in each of the climatic zones over the study site, based on the aridity index (AI: ratio between precipitation and potential evapotranspiration) (Hyper Arid: AI <0.03, Arid: 0.03 < AI <0.2, Semi-Arid: 0.2 < AI <0.5, Dry sub-humid: 0.5 < AI <0.65, and Humid: AI >0.65) (UNEP, 1992). For this comparison, the ratio between model fluxes and precipitation was calculated for each behavioural simulation. Areas for each aridity class were calculated for each precipitation dataset, thus, each model outputs in a different climatological distribution depending on the precipitation dataset. Fluxes for each aridity class were spatially aggregated by averaging all cells within the climatic zone before the normalization.

3 | RESULTS

3.1 | Comparisons between simulated and observed hydrological variables

The calibration of DRYP resulted in 54, 31, and 95 behavioural models, as solely based on streamflow at Archer's Post, for MSWEP, IMERG, and ERA, respectively. At the catchment outlet, the best models produced values of KGE of ~0.65 and PBIAS of ~6% for the MSWEP forcing dataset, KGE of ~0.68 and PBIAS of ~7%, for the IMERG dataset, and KGE of ~0.66 and PBIAS of −1.7% for ERA-forced models. Given the complex hydrological conditions of the basin and the large-scale gridded datasets used to force the hydrological

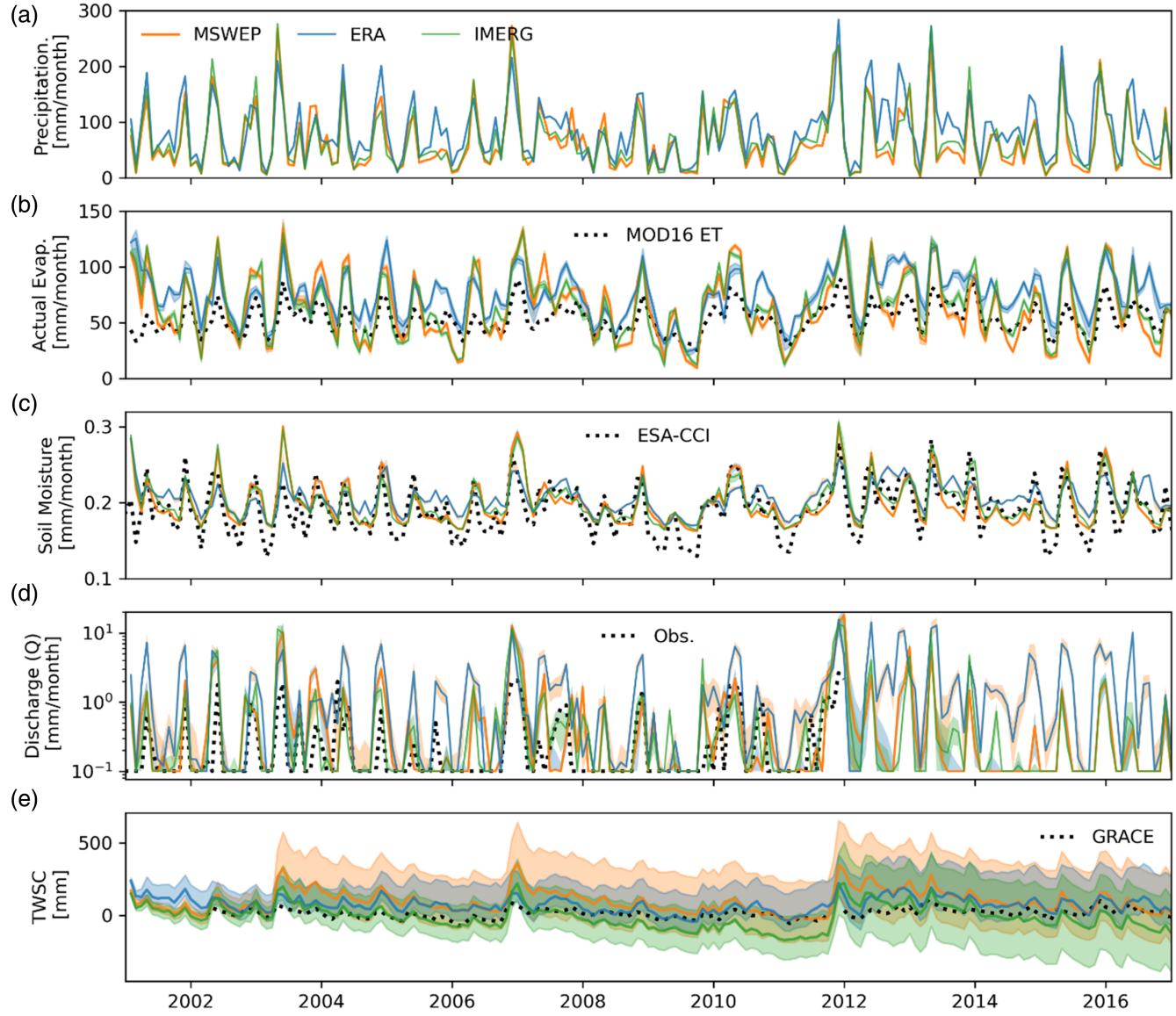

FIGURE 2 Monthly temporal variation over the whole basin: (a) precipitation, (b) actual evapotranspiration (MOD16 ET), (c) soil moisture (ESA-CCI, (d) observed discharge at the catchment outlet (Archer's Post, see Figure 1), and (e) change in total water storage change, TWSC (GRACE). Shaded area represents the 95% uncertainty interval estimated from all behavioural models.

model (Bain et al., 2023; Barkhordari et al., 2023; Beck et al., 2020; Satgé et al., 2021), these evaluation results suggest that calibrated DRYP models are skilful at simulating streamflow at the catchment outlet of the Ewaso Ng'iro basin.

The calibrated DRYP models well capture the temporal variation of streamflow at the basin outlet (Archer's post, Figure 1a) for all three forcing datasets (Figure 2d), for example, during the large flow events in March 2003, December 2007 and December 2012, although they fail to well capture other flow events (e.g., December 2004, March 2010). Overall, there are high correlations between modelled and measured streamflow for all rainfall forcing datasets (Q_{MSWEP}: $r = 0.70$, $p < 0.001$; Q_{ERA}: $r = 0.78$, $p < 0.001$, and Q_{IMERG}: $r = 0.74$, $p < 0.001$). However, for smaller flow peaks, model runs forced by both MSWEP and IMERG tend to underestimate monthly streamflow values, whereas the ERA runs overestimate medium and low values. The MSWEP dataset shows the best performance when only the KGE statistic is considered, yet the ERA dataset performs best when considering both PBIAS and KGE. Overall, the results thus demonstrate that the DRYP model can simulate the production of catchment runoff and its delivery to streams despite its inherent parsimony and simplicity, irrespective of the choice of forcing precipitation and PET datasets.

Regardless of forcing precipitation data, the behavioural models also capture well the monthly fluctuations in AET, soil moisture, streamflow, and changes in TWS over the whole basin (Figure 2), based on evaluation against MOD16 ET, ESA-CCI soil moisture, observed streamflow, and GRACE-TWS, respectively. For example, there is high correlation between monthly average values of modelled

AET and MOD16 ET (Figure S3a, $AET_{MSWEP/MOD16ET}$: $r = 0.81$, $p < 0.001$; $AET_{ERA/MOD16ET}$: $r = 0.85$, $p < 0.001$; and $AET_{IMERG/MOD16ET}$: $r = 0.82$, $p < 0.001$). Similarly, temporal fluctuations in modelled soil moisture for all precipitation forcing datasets compare well with ESA-CCI (Figure 2c, $SM_{MSWEP/ESA-CCI}$: $r = 0.69$, $p < 0.001$; $SM_{ERA/ESA-CCI}$: $r = 0.80$, $p < 0.001$, and $SM_{IMERG/ESA-CCI}$: $r = 0.77$, $p < 0.001$). The contributions of modelled diffuse and focused recharge and soil water content result in a good representation of modelled total water storage changes compared with GRACE TWSC (Figure 2e), despite the small basin size of the Ewaso Ng'iro (~15 700 km^2) compared to the GRACE mascon size. We found significant correlation for all precipitation forcing datasets ($TWSC_{MSWEP/GRACE}$: $r = 0.52$, $p < 0.001$, $TWSC_{ERA/GRACE}$: $r = 0.565$, $p < 0.001$, and $TWSC_{IMERG/GRACE}$: $r = 0.59$, $p < 0.001$). However, it should be noted that the model simulations consistently show larger fluctuations than the GRACE TWSC dataset, which can be attributed to the high spatial resolution of the model domain compared to the GRACE dataset.

Spatially, mean annual outputs from all behavioural models for each precipitation forcing dataset showed larger areas with good spatial correlation in modelled AET and soil moisture when compared to MOD16 ET (Figure S3a), and ESA-CCI (Figure S3c) datasets, respectively. For AET, mean annual values for all three models show moderate to strong positive correlation ($r > 0.6$) in semi-arid areas (Figure S3a) but low and negative correlation in humid areas, particularly around Mount Kenya. Similarly, a positive (>0.5) for most of the model domain was also obtained for mean modelled soil moisture in relation to the ESA-CCI dataset (Figure S3b). The results also show a decrease in performance in humid areas of the southern (Mt. Kenya) and the northeast parts of the basin (Figure S3b).

3.2 | Spatial variability between gridded precipitation datasets

A summary of the variability of yearly precipitation across the area is shown in Table 4 and in the supplemental material. These data have also been disaggregated according to different aridity classes (Figure 3b) (Table 3). This analysis shows that the ERA data has a much larger total precipitation than IMERG and MSWEP (highest values of mean annual precipitation in ERA are ~2020 mm y^{-1}), and this feature is accentuated in the humid parts of the basin. Additionally, ERA is the only dataset that shows arid conditions (AI <0.2) anywhere in the basin (Figure S5), while mean annual precipitation is the highest in semi-arid and sub-humid areas for the IMERG dataset.

3.3 | Long term variability of water balance components to precipitation datasets

A summary of the estimated long-term average water balance fluxes for the basin from all behavioural models is shown in Table 5. Overall, the analysis shows that AET from the soil is the main mechanism of water losses from the basin (>720 mm y^{-1}). For all models, AET has very similar values despite the difference between the precipitation datasets (Tables 4 and 5). However, AET output from ERA-forced models shows more uncertainty indicated by much higher variability in long term average annual values between behavioural models (std ~24 mm y^{-1}) than the other two datasets (std. ~10.0 mm y^{-1} for both MSWEP and IMERG). AET from riparian areas has nearly identical values for all datasets, also with low uncertainty (std. <1.1 mm y^{-1}).

However, large differences arise between ERA and the other two datasets MSWEP and IMERG for the rest of the water balance components. For instance, for overland flow, ERA-calibrated models showed the highest value (~94 mm y^{-1}), followed by IMERG (~50 mm y^{-1}), and then by MSWEP (~39 mm y^{-1}), despite the latter two having very similar annual precipitation. Models forced by MSWEP and IMERG have similar values of transmission losses (MSWEP: ~21 mm y^{-1}; IMERG: 24 mm y^{-1}), and focused recharge. However, these values differ considerably from those generated by ERA-forced models for transmission losses and focused recharge. A similar pattern of divergence is also seen for diffuse recharge and groundwater boundary flow (BC), with much larger estimations of both components for ERA than both MSWEP and IMERG. IMERG models show higher values of BC than MSWEP models despite both having similar annual precipitation rates. However, the low values of BC for MSWEP models are compensated with high values of AET_{GW} (~15 mm y^{-1}). The highest values of BC and AET_{GW} for ERA models compensate the highest annual precipitation rates of this dataset.

The analysis shows that the higher precipitation rates within the ERA dataset are propagated through all fluxes of the Ewaso water

TABLE 4 Spatial variability of precipitation and area within AI classes covered by each precipitation dataset (additional information provided in Figure S3).

	Total	Arid (AI <0.2)		Semi-arid (0.5 < AI <0.5)		Sub-humid (0.5 < AI <0.65)		Humid (AI >0.65)	
	Precip.*	Precip.*	Area	Precip.*	Area	Precip.*	Area	Precip.*	Area
Dataset	mm y^{-1}	mm y^{-1}	%	mm y^{-1}	%	mm y^{-1}	%	mm y^{-1}	%
IMERG	794 (182)	0 (0)	0	732 (134)	79	1021 (64)	19	1249 (107)	2
MSWEP	800 (225)	0 (0)	0	602 (82)	79	855 (71)	10	1234 (196)	11
ERA	950 (718)	347 (47)	17	658 (149)	48	1088 (108)	9	2020 (620)	26

*Values in brackets are the standard deviation.

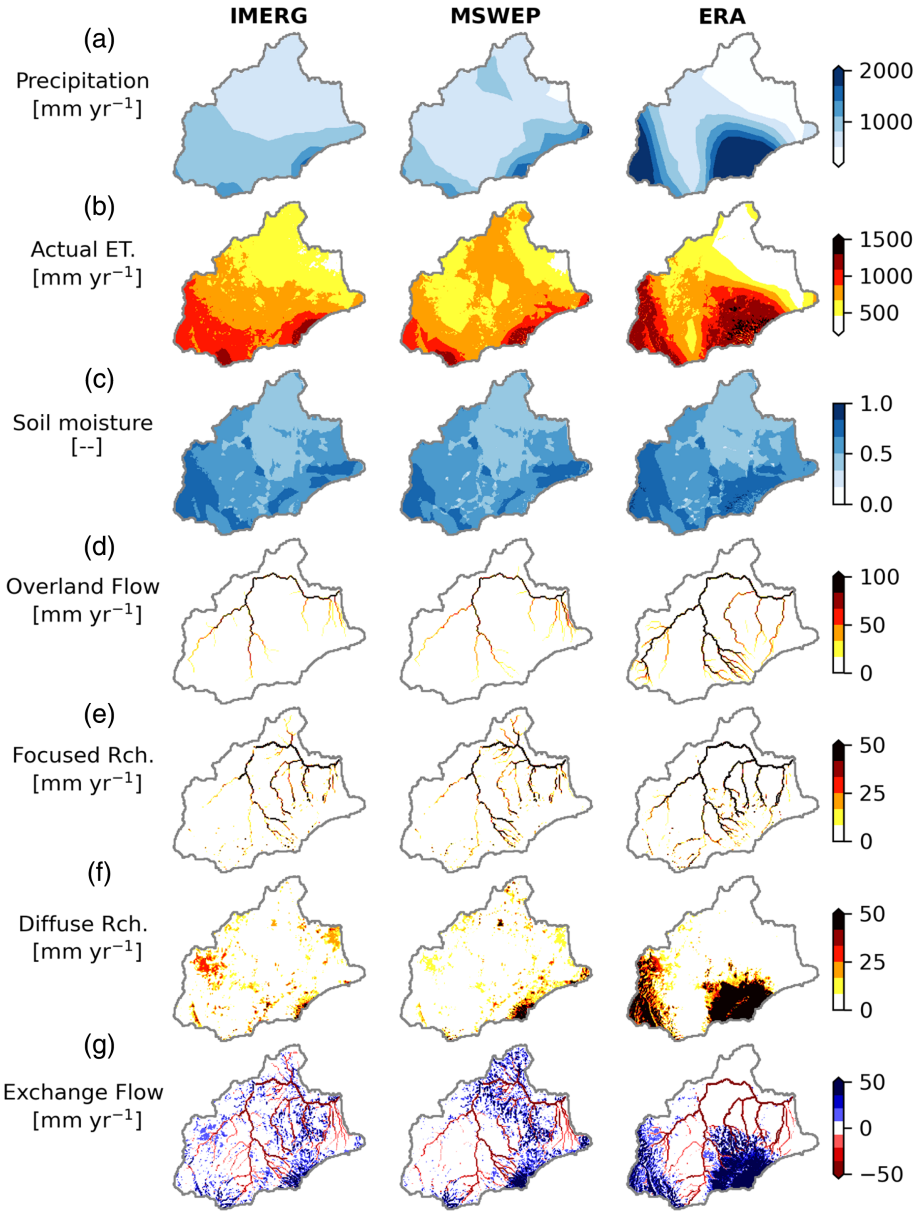

FIGURE 3 Mean values of yearly fluxes from all behavioural simulations for each of the precipitation forcing datasets, ERA, IMERG, and MSWEP: (a) Precipitation, (b) Actual evapotranspiration, (c) soil moisture, (d) overland flow, (e) focused recharge, (f) diffuse recharge, and (g) flow exchange (baseflow – transmission losses).

balance, although it has less influence on AET. The amount of AET in humid areas of the basin depends on the PET and the capacity of the unsaturated zone to store water. Therefore, since the PET is kept equal for all model experiments and since annual rates of precipitation vary most significantly in humid areas for all three datasets (Table 4), this is to be expected. In riparian areas of the basin, transmission losses provide additional water to the streambed in comparison to non-riparian areas, so there is more available water to be returned to the atmosphere and water can be evaporated at the full potential rate for much longer periods of time (Table 4).

ERA-forced modelled fluxes also have larger uncertainty, represented by the high standard deviation between behavioural simulations, in relation to the other datasets. The absolute magnitude of these uncertainties values seems to be associated to the magnitude of mean values, with large mean fluxes showing large uncertainties (e.g., TL_{ERA}: coefficient of variation ~0.30, whereas TL_{IMERG} and TL_{MSWEP} have coefficients of variation of ~0.34 and ~ 0.33, respectively).

3.4 | Spatial variability of water balance components to forcing precipitation datasets

Figure 3 shows mean annual values of selected components of the water balance estimated for each precipitation dataset, characterizing the hydrological response to precipitation forcing. The uncertainty of these fluxes and state variables are shown in Figure S6. For all the water balance components presented in Figure 3, there is a marked difference between models for the different precipitation forcing datasets.

For AET, all datasets follow the spatial distribution of precipitation, with the highest rates of AET concentrated in humid areas

TABLE 5 Yearly mean and standard deviation (parentheses) long-term average components of the water balance for the Upper Ewaso Ng'iro basin; all values were estimated using all behavioural simulations for the three forcing datasets: MSWEP, ERA, and IMERG.

	Forcing dataset		
	IMERG	MSWEP	ERA
Flux	Mean (Std.) [mm y^{-1}]	Mean (Std.) [mm y^{-1}]	Mean (Std.) [mm y^{-1}]
Precipitation (*P*)	794	800	950
Infiltration (*I*)	749 (8)	755 (7)	858 (17)
Actual Evapotranspiration (AET)	728 (10)	723 (10)	738 (24)
Riparian evapotranspiration (AET_{RP})	5 (1)	5 (1)	5 (1)
Overland flow (OF)	50 (8)	39 (7)	94 (17)
Transmission losses (TL)	24 (8)	21 (7)	105 (32)
Diffuse recharge (R_{dif})	21 (2)	32 (3)	120 (7)
Focused recharge (R_{foc})	19 (7)	16 (6)	100 (31)
Streamflow (*Q*)	35 (4)	35 (4)	42 (7)
Baseflow (BF)	9 (4)	18 (4)	54 (22)
Groundwater flow at boundary (BC)	30 (11)	15 (8)	147 (41)
Capillary rise (AET_{GW})	1 (1)	15 (3)	19 (3)

(Figure 3b, Figure S7), although these areas are also characterized by high uncertainty in AET (Figure S7). AET at humid and high-altitude areas is expected to be limited only by energy demands from the atmosphere (no water limitation). Therefore, in these areas the maximum amount of AET equals the rate of PET. In the case of soil moisture, there is low variability between the three datasets, yet their spatial distribution is mostly consistent with the spatial distribution of precipitation (Figure 3b). The uncertainty in soil moisture from all behavioural models is also high in areas where precipitation is high (Figure S6b). For overland flow, there are marked differences between all three datasets (Figure 3c). For ERA-forced output, high rates of streamflow extend from humid and high elevation areas of the basin, whereas for IMERG and MSWEP, high streamflow occurs farther away from the humid areas. This indicates that the partitioning of the higher rates of precipitation into runoff and infiltration for ERA-forced models is in part propagated into overland flow. Focused recharge follows the same pattern as runoff (Figure 3e), with ERA-forced output also widely distributed over the basin and higher rates occurring at higher elevations in comparison to IMERG and MSWEP. Overland flow and focused recharge are shown to increase in lowland areas, which is consistent with the expected cumulative effect of the flow routing mechanism. Diffuse recharge, on the other hand, behaves in the opposite manner to focused recharge. Diffuse recharge is mostly concentrated in humid areas where annual precipitation is also high and, therefore, it follows a similar spatial distribution to precipitation (Figure 3e). Finally, Figure 3f shows the spatial distribution of groundwater-surface water exchange resulting from the difference between groundwater discharge and recharge, with positive values indicating water discharging from the aquifer, while negative values represent aquifer recharge. The distribution of groundwater discharge for all models generally follows the precipitation distribution with high discharge rates occurring in humid areas. However, groundwater is also discharged at mountain flanks of low, more arid areas.

Figure 4 illustrates the variability of selected components of the water balance across different elevations. In general, models forced with IMERG and MSWEP show similar values across the elevation gradient for the selected fluxes. However, this pattern significantly differs for ERA-forced models, where the high precipitation gradient results in considerably higher values of infiltration (Figure 4b) and diffuse recharge (Figure 4f) at higher elevations. Additionally, the increased precipitation at higher elevations (>3000 m) translates into transmission losses (Figure 4d) and focused recharge (Figure 4e) in lowland areas. AET values for the three datasets remain consistent across elevations, although higher rates are observed at mid elevations (2000–2800 m) for the ERA dataset. These elevational differences in AET are reasonable since water-limited conditions are not met in the uplands where more water is available for evaporation based on the ERA dataset at mid-elevations due to its higher precipitation.

3.5 | Variability of water balance partitioning across climatic zones

Figure 4 shows AET, diffuse and focused recharge for each forcing dataset and for the aridity index classes. The differences between the normalized fluxes of each dataset represent the influence of the variability in the magnitude of the precipitation on each AI class.

In general, Figure 5 highlights the increased influence of water losses through AET as aridity increases. The switch from energy to water limited conditions, already explained in previous sections, are the main mechanisms that control this process. In contrast, diffuse

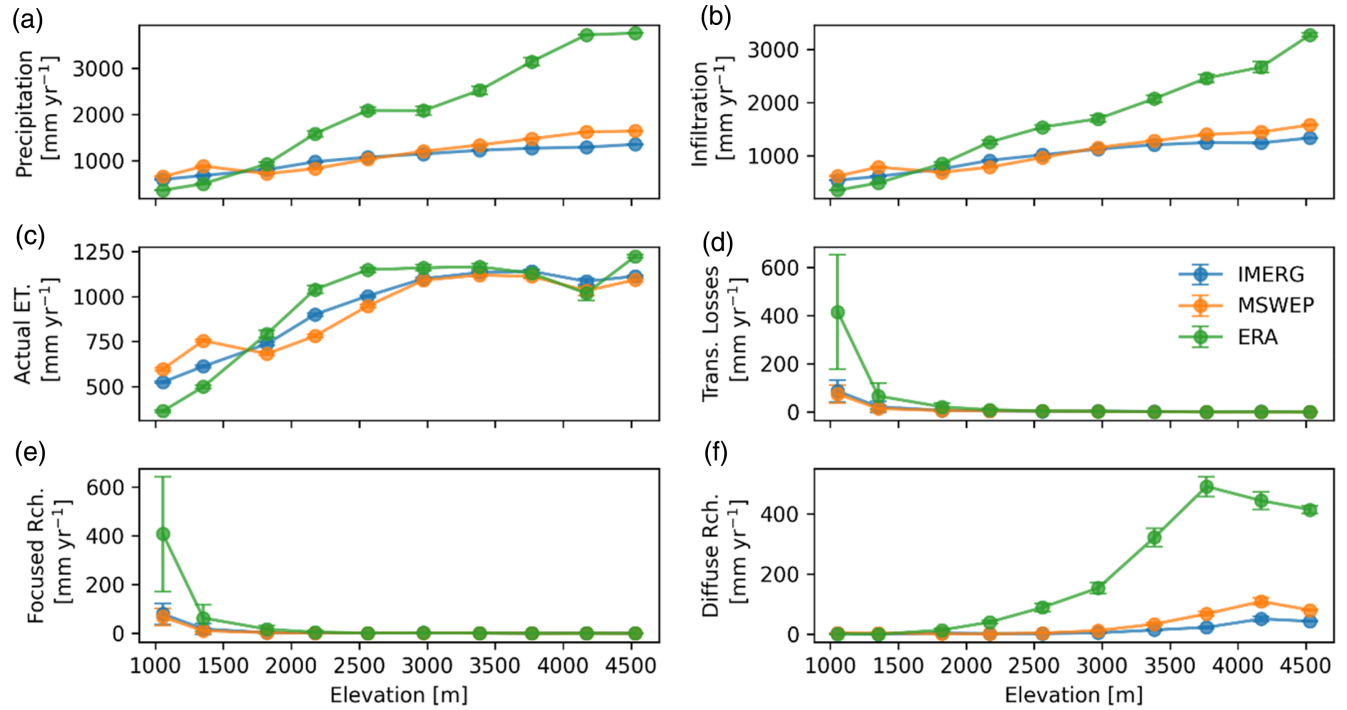

FIGURE 4 Variation of mean annual values of hydrological fluxes against elevation for: (a) precipitation, (b) infiltration, (c) actual evapotranspiration, (d) transmission losses, (e) focused recharge, and (f) diffuse recharge. Mean annual values of each flux across the entire model domain were grouped into elevation ranges of 400 m. Error bars represent the standard deviation, but the size of error bars has been reduced 10-fold to improve the visualization.

recharge decreases as aridity increases, with less diffuse recharge occurring in arid and semi-arid areas for all datasets (Figure 5d–f). ERA-forced models which have the highest values of precipitation in humid areas also show the highest values (~15.8%) of normalized diffused recharge in comparison to both IMERG (~2.5%) and MSWEP (~5.5%). Thus, the highest rates of precipitation are propagated into the diffuse recharge of humid areas. It can also be seen that despite both IMERG and MSWEP datasets having similar mean annual values of precipitation in humid areas, normalized values of diffuse recharge differ for both models. This can be attributed to the spatial variability of precipitation over the humid area, with higher precipitation rates and larger humid areas for the MSWEP dataset in comparison to IMERG (see Figure S2, Table 4).

The opposite happens with normalized focused recharge, where higher values are observed in semi-arid and sub-humid areas (Figure 5g,h) in comparison to humid areas (Figure 5i). Models capture the increasing influence of focused recharge in increasingly arid areas of the basin. Results also reflect that for higher precipitation rates (e.g., in ERA), DRYP propagates those high rates into focused recharge, which in turn becomes the main source of aquifer recharge in arid and semi-arid areas. Similar results are shown for both MSWEP and IMERG where the normalized values also increase in drier areas.

Figure 6 shows how recharge components (diffuse (a) and focused (b)) and total recharge (c) vary with mean annual precipitation (MAP) rates. As expected, diffuse recharge increases as MAP increases, and this trend across different precipitation ranges follows a similar pattern of long-term annual groundwater recharge values (LTAR) compared to precipitation totals documented for the entire African continent by (MacDonald et al., 2021). Diffuse recharge decreases under dry conditions for all datasets (Figure 6). It can also be seen that our model generally produces lower values in comparison to LTAR although the range of variation in LTAR (error bars represent 1-standard deviation) is also high and increases with MAP. Both, IMERG and MSWEP systematically underestimate diffuse recharge for precipitation rates above 400 mm y^{-1} when compared to values reported in the literature (LTAR, MacDonald et al. (2021)). The ERA dataset seems to produce similar values of diffuse recharge ($DRYP_{ERA}$: ~400 mm y^{-1}, LTAR: ~400 mm y^{-1}) for precipitation rates above 1400 mm y^{-1}. However, below 1400 mm y^{-1}, ERA shows similar values of diffuse recharge to both IMERG and MSWEP. The opposite pattern occurs with modelled focused recharge, which decreases with rising MAP. The range of variation for simulated focused recharge is also high but it decreases considerably with MAP. It can also be seen that the highest values of focused recharge are considerable higher than the corresponding values of MAP. These high values of recharge mainly occur in lowland areas (Figure 3), indicating that the main source of focused recharge is runoff coming from upland areas. Figure 6c clearly illustrates the increasing contribution of focused recharge to the total groundwater recharge as the precipitation declines in arid parts of the basin. In the case of focused recharge, ERA and MSWEP shows more consistent results between these two datasets for all ranges of precipitation rates, but they differ with the

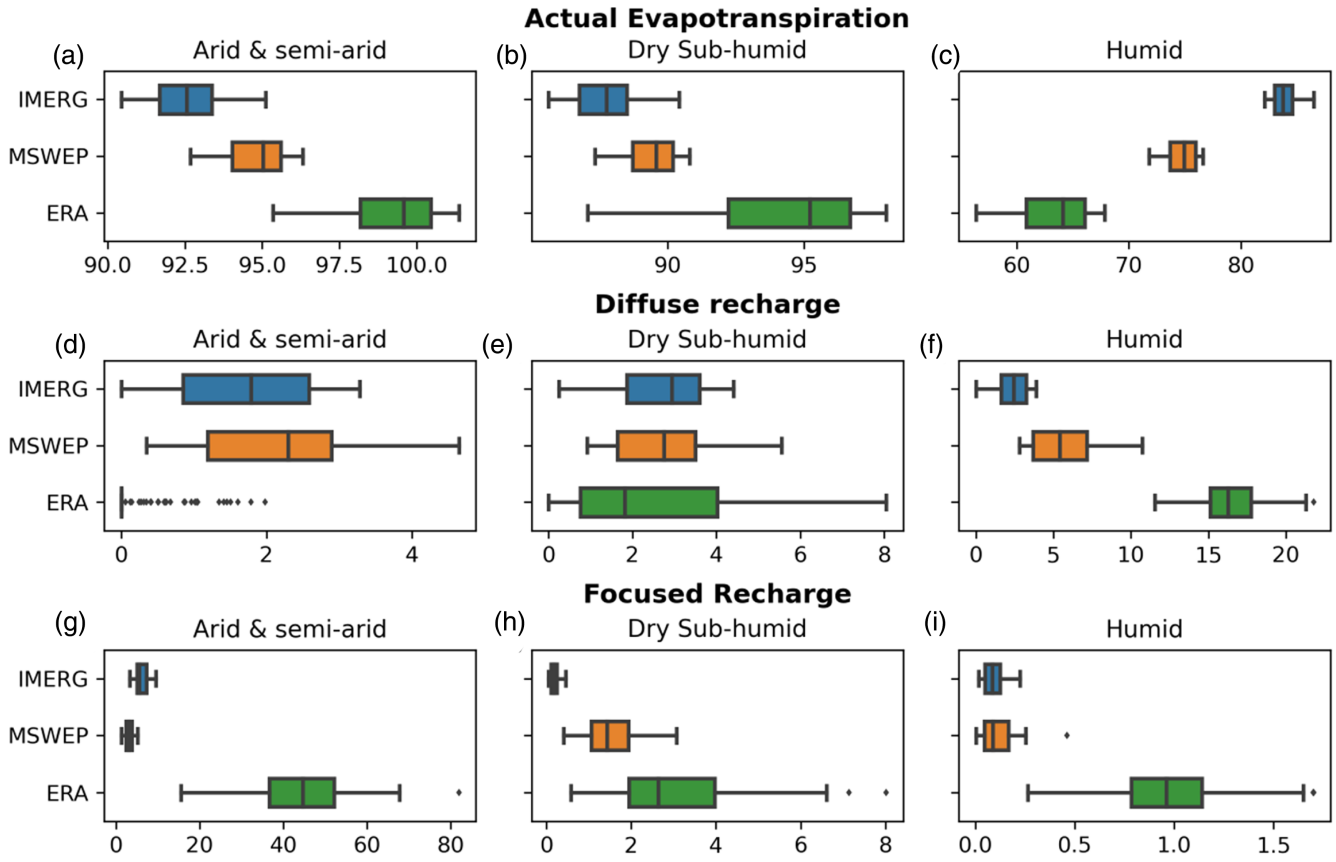

FIGURE 5 Uncertainty of water fluxes normalized by precipitation using all behavioural models for each climatological zone: actual evapotranspiration from all sources (AET_{UZ}, AET_{RUZ}, and AET_{GW}) for arid and semi-arid (a), dry sub-humid (b), and humid zones (c); focused recharge for arid and semi-arid (d), dry sub-humid (e), humid zones (f); and diffuse recharge for arid and semi-arid (g), dry sub-humid (h), and humid zones (i). Estimates correspond to mean yearly values.

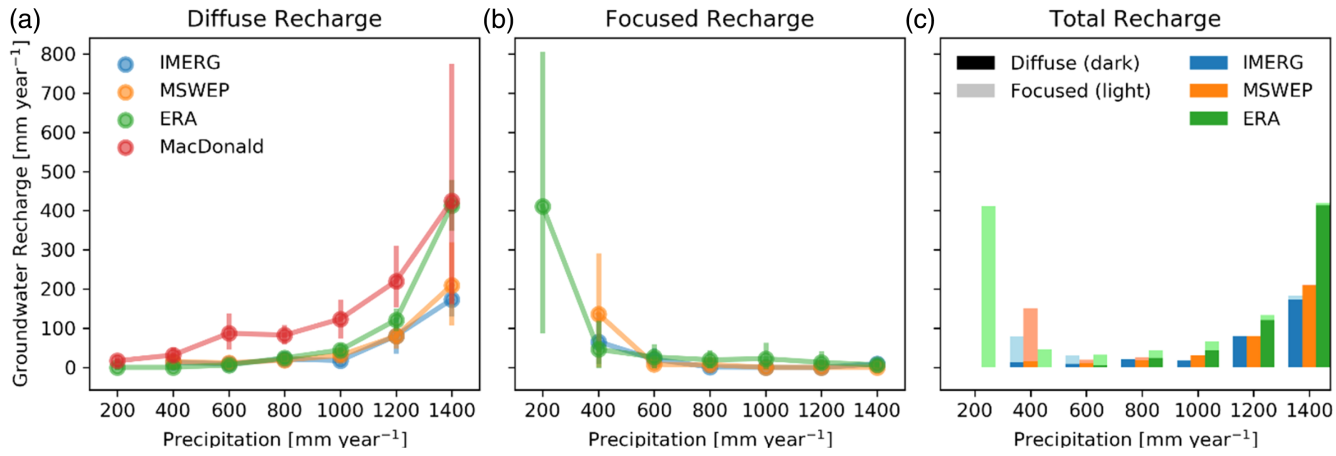

FIGURE 6 Variation of groundwater recharge components in relation to mean annual precipitation (MAP): (a) Diffuse recharge, (b) Focused recharge, and (c) Total recharge (Diffuse + Focused). Values of recharge corresponds to average of mean yearly values of all behavioural simulations. Values of precipitation are binned in 200 mm y^{-1} bins. Error bars correspond to the standard deviation of all cells falling in each bin. Light colours in bar plot correspond to focused recharge, whereas dark colours diffuse recharge.

IMERG dataset at precipitation rates of 600 mm y^{-1}, range at which IMERG has the highest values (IMERG: ~150 mm y^{-1}, MSWEP: ~92 mm y^{-1}, and ERA: ~90 mm y^{-1}). It can also be seen that ERA shows considerably high values of focused recharge (~405 mm y^{-1}) at the lowest precipitation rates (~200 mm y^{-1}) appearing only in this dataset.

4 | DISCUSSION

The analysis shows that the choice of input precipitation dataset has important implications for the spatial distribution and temporal variability of water balance components (Figure 3). In general, the ERA dataset shows significantly higher precipitation values in humid areas, whereas IMERG and MSWEP have more consistent values across the model domain. It is important to highlight that the ERA re-analysis gridded datasets have been found to under-perform at high elevations, with a positive bias increasing with elevation (Jiao et al., 2021). Despite spatial and temporal differences between the three datasets, they produce behavioural simulations that effectively capture the temporal variation of specific water balance components, such as streamflow, soil moisture, actual evapotranspiration, and total water storage change. This performance was evaluated against streamflow observations and the corresponding remote sensing data (Figure 2). The ERA dataset shows significantly higher magnitudes of transmission losses and focused recharge estimates than the other two datasets.

Differences in components such as transmission losses, groundwater recharge, and outflow through basin boundary (see Table 4) may suggest that precipitation variability has a greater impact on water partitioning than model calibration. To close the water balance of the basin, the calibration makes mainly a tread-off of unconstrained components by increasing or decreasing their magnitude. For example, for the ERA dataset, fluxes, such as transmission losses and baseflow become more relevant in comparison to outflow as streamflow at the catchment outlet, whereas the opposite occurs for IMERG and MSWEP datasets (see Table 4). These differences have important implications when assessing the availability of water resources since the choice of precipitation dataset may show great spatial and temporal differences on water fluxes within the study area.

The hydrological fluxes estimated in the Ewaso Ng'iro basin show greater consistency with the IMERG and MSWEP datasets compared to the ERA dataset. For instance, AET accounts for over 90% of total precipitation in both the MSWEP and IMERG datasets, whereas in the ERA dataset, this percentage drops to around 78%. These percentages vary significantly based on climatic conditions (Figure 5a–c). In humid areas, where AET operates under energy-limited conditions, the variability in precipitation has less impact on estimated AET rates because evaporation occurs at potential evapotranspiration rates (Budyko, 1961; Gudmundsson et al., 2016; Padrón et al., 2017). Conversely, in arid regions, where AET is primarily water-limited, it becomes more sensitive to precipitation variability. In this context, having more consistent precipitation datasets for arid and semiarid areas would greatly improve water partitioning quantification in these regions. In the case of humid areas, it is essential to assess how the variability in PET may influence AET estimations.

Groundwater recharge also exhibits significant differences between the datasets. On one hand, for precipitation rates >1200 mm y^{-1} (corresponding to humid areas), the ERA dataset shows more consistent values for diffuse recharge compared to the LTAR dataset (Figure 6). This suggests that diffuse recharge estimations are sensitive to higher precipitation rates, but it also raises the possibility that IMERG and MSWEP precipitation datasets might underestimate precipitation within humid areas. On the other hand, focused recharge also shows differences, particularly in the more arid areas where precipitation rates are lower (Figure 6). Despite the variations between datasets, the model results align broadly with the expected mechanisms governing diffuse and focused recharge, as supported by previous field observations in predominantly dry climatic conditions (Cuthbert et al., 2019; MacDonald et al., 2021).

Finally, the variability between precipitation datasets characterized by differences in precipitation gradients (see Figure 3 and Table 4) also impacts the uncertainty of model estimates for water balance components. As shown in Table 4, the ERA dataset, which exhibits the highest rates of precipitation results in wider ranges of fluxes, compared to other datasets (see Figure 5). This, in addition to the substantial differences between the water balance components indicates that a careful consideration of estimated flux magnitudes is essential due to the high uncertainty (Figure 5 and S2). Reducing this uncertainty will require more accurate information as well as the incorporation of more evaluation datasets such as water table depth or streamflow at different locations within the model. This will help to constrain water balance components that are not possible to be directly evaluated.

5 | CONCLUSION

The present study analysed the influence of the spatial and temporal variability of precipitation forcing datasets on water partitioning of the Upper Ewaso Ng'iro basin using a dryland hydrological model (DRYP). Three precipitation datasets with high spatial and temporal resolution, IMERG, ERA and MSWEP, were used for the analysis. The model was evaluated against flux and storage observations from remote sensing datasets (ESA, MOD16 ET, and GRACE) and streamflow observations available at the catchment outlet. Overall, results show good performance of the model in representing soil moisture, actual evapotranspiration, total water storage and streamflow. Based on the analysis, the following conclusions can be drawn.

Spatial and temporal variability within each precipitation dataset results in high variability in water balance components for the Upper Ewaso Ng'iro basin. For each dataset, the spatial distribution of fluxes and hydrological states are consistent with the spatial distribution of the precipitation dataset. Precipitation datasets exhibiting higher precipitation gradients with elevation, such as the ERA dataset, produce larger ranges of variation of transmission losses, as well as diffuse and focused recharge. Actual evapotranspiration is consistent for all forcing datasets with water limited and energy limited conditions controlling the rates of actual evapotranspiration in arid and semi-arid, and humid areas, respectively.

The spatial and temporal variability within precipitation datasets also affect the uncertainty of hydrological fluxes. The forcing dataset with the highest spatial precipitation gradient results in wider ranges of infiltration, actual evapotranspiration, transmission losses, and

focused recharge. More accurate representation of the spatial and temporal variability of precipitation of gridded datasets is required to reduce the uncertainty of water balance components. In turn, this will result in more consistent estimates of the spatial variability of water balance components over the basin.

In the Upper Ewaso Ng'iro basin, the three precipitation datasets showed relatively similar performance across the evaluated metrics of soil moisture, actual evapotranspiration, total water storage anomalies, and streamflow. Among these datasets, the ERA precipitation dataset showed the best performance for representing actual evapotranspiration ($r = 0.78$) and soil moisture ($r = 0.85$). MSWEP showed the best performance for representing streamflow (KGE = 0.68), whereas IMERG showed the best performance in representing TWSA ($r = 0.59$). These variations in performance across specific variables suggest that each dataset contains relevant information related to the evaluated variables.

Finally, considering the variability of forcing datasets, exploring a broader range of spatial and temporal variability in precipitation and potential evapotranspiration for quantifying water partitioning will also aid in reducing uncertainty. Utilizing tools to explore the stochastic behaviour of forcing datasets (e.g., stoPET v1.0 Asfaw et al. (2023), STORM (Rios Gaona et al., 2023; Singer et al., 2018) will help understand how the variability in forcing datasets impacts different components of the water balance, thereby improving model estimations. This, in turn, will enhance our understanding of the influence of climate change variability on surface and subsurface water balance components, particularly groundwater. Addressing the high uncertainty of current estimations regarding the effects of climate change on groundwater (IPCC6, 2021), is crucial, especially in water-scarce dryland regions.

ACKNOWLEDGEMENTS

E. Andrés Quichimbo received financial support from Cardiff University through a Vice Chancellor's Scholarship. Mark O. Cuthbert gratefully acknowledges funding for an Independent Research Fellowship from the UK Natural Environment Research Council (grant no. NE/P017819/1). Michael Bliss Singer has been supported by the U.S. National Science Foundation (grant nos. BCS-1660490 and EAR-1700555) and the U.S. Department of Defence's Strategic Environmental Research and Development Program (grant no. RC18-1006). Rafael Rosolem has been supported by the Natural Environment Research Council (NERC), under the MOSAIC Digital Environment Feasibility Study (grant no. NE/T005645/1), and by the International Atomic Energy Agency of the United Nations (IAEA/UN; project no. CRP D12014). The team has been supported by the Global Challenges Research Fund (GCRF; "Impacts of Climate Change on the Water Balance in East African Drylands"), The Royal Society ("DRIER", grant no. CHL\R1\180485), and the European Union's Horizon 2020 programme ("DOWN2EARTH", grant no. 869550)

DATA AVAILABILITY STATEMENT

The DRYPv1.0 code is available at https://github.com/AndresQuichimbo/DRYP (last access: 10 October 2021). Our dataset contains modified Copernicus Climate Change Service information (1981–present) available at https://cds.climate.copernicus.eu/cdsapp#!/dataset/reanalysis-era5-single-levels?tab=form (European Centre for Medium-Range Weather Forecasts, 2018). Precipitation for each dataset is publicly available at: MSWEP: www.gloh2o.org (last accessed: 20/11/2021). IMERG: https://gpm1.gesdisc.eosdis.nasa.gov/ (last accessed: 20/11/2021). ERA5: https://cds.climate.copernicus.eu/cdsapp#!/dataset/reanalysis-era5-single-levels?tab=form (last accessed: 20/02/2022). hPET is publicly available at: https://doi.org/10.5523/bris.qb8ujazzda0s2aykkv0oq0ctp (last accessed: 01/12/2021). The streamflow dataset used in this research is publicly available at https://wlrc-ken.org/data/timeseries/index. The soil moisture dataset is publicly available at https://lpdaac.usgs.gov/products/mod16a2v006/. GRACE total water storage anomalies are publicly available at http://grace.jpl.nasa.gov.

ORCID

M. B. Singer https://orcid.org/0000-0002-6899-2224

REFERENCES

Abdulrazzak, M. J. (1995). Losses of flood water from alluvial channels. *Arid Soil Research and Rehabilitation*, *9*, 15–24. https://doi.org/10.1080/15324989509385870

Aguilar, A. L., Flores, H., Crespo, G., Marín, M. I., Campos, I., & Calera, A. (2018). Performance assessment of MOD16 in evapotranspiration evaluation in northwestern Mexico. *Water*, *10*, 901. https://doi.org/10.3390/w10070901

Alexander, L. V., Bador, M., Roca, R., Contractor, S., Donat, M. G., & Nguyen, P. L. (2020). Intercomparison of annual precipitation indices and extremes over global land areas from in situ, space-based and reanalysis products. *Environmental Research Letters*, *15*, 055002. https://doi.org/10.1088/1748-9326/ab79e2

Aryal, S. K., Silberstein, R. P., Fu, G., Hodgson, G., Charles, S. P., & McFarlane, D. (2020). Understanding spatio-temporal rainfall-runoff changes in a semi-arid region. *Hydrological Processes*, *34*, 2510–2530. https://doi.org/10.1002/hyp.13744

Asfaw, D. T., Singer, M. B., Rosolem, R., MacLeod, D., Cuthbert, M., Miguitama, E. Q., Rios Gaona, M. F., & Michaelides, K. (2023). stoPET v1.0: A stochastic potential evapotranspiration generator for simulation of climate change impacts. *Geoscientific Model Development*, *16*, 557–571. https://doi.org/10.5194/gmd-16-557-2023

Ayugi, B., Tan, G., Ullah, W., Boiyo, R., & Ongoma, V. (2019). Intercomparison of remotely sensed precipitation datasets over Kenya during 1998–2016. *Atmospheric Research*, *225*, 96–109. https://doi.org/10.1016/j.atmosres.2019.03.032

Bain, R. L., Shaw, M. J., Geheran, M. P., Tavakoly, A. A., Wahl, M. D., & Zsoter, E. (2023). Intercomparison of global ERA reanalysis products for streamflow simulations at the high-resolution continental scale. *Journal of Hydrology*, *616*, 128624. https://doi.org/10.1016/j.jhydrol.2022.128624

Barkhordari, H., Nasseri, M., & Rezazadeh, H. (2023). Possibility of global gridded streamflow dataset correction: Applications of large-scale watersheds with different climates. *Theoretical and Applied Climatology*, *152*, 627–647. https://doi.org/10.1007/s00704-023-04388-2

Beck, H. E., Pan, M., Lin, P., Seibert, J., van Dijk, A. I. J. M., & Wood, E. F. (2020). Global fully distributed parameter regionalization based on observed streamflow from 4,229 headwater catchments. *Journal of Geophysical Research Atmospheres*, *125*, e2019JD031485. https://doi.org/10.1029/2019JD031485

Beck, H. E., Vergopolan, N., Pan, M., Levizzani, V., van Dijk, A. I. J. M., Weedon, G. P., Brocca, L., Pappenberger, F., Huffman, G. J., &

Wood, E. F. (2017). Global-scale evaluation of 22 precipitation datasets using gauge observations and hydrological modeling. *Hydrology and Earth System Sciences*, *21*, 6201–6217. https://doi.org/10.5194/hess-21-6201-2017

Beck, H. E., Wood, E. F., Pan, M., Fisher, C. K., Miralles, D. G., van Dijk, A. I. J. M., McVicar, T. R., & Adler, R. F. (2019). MSWEP V2 global 3-hourly 0.1° precipitation: Methodology and quantitative assessment. *Bulletin of the American Meteorological Society*, *100*, 473–500. https://doi.org/10.1175/BAMS-D-17-0138.1

Bianchi, M., MacDonald, A. M., Macdonald, D. M. J., & Asare, E. B. (2020). Investigating the productivity and sustainability of weathered basement aquifers in tropical Africa using numerical simulation and global sensitivity analysis. *Water Resources Research*, *56*, e2020WR027746. https://doi.org/10.1029/2020WR027746

Bitew, M., Gebremichael, M., Ghebremichael, L., & Bayissa, Y. (2012). Evaluation of high-resolution satellite rainfall products through streamflow simulation in a hydrological modeling of a small mountainous watershed in Ethiopia. *Journal of Hydrometeorology*, *13*, 338–350. https://doi.org/10.1175/2011JHM1292.1

Blatchford, M. L., Mannaerts, C. M., Njuki, S. M., Nouri, H., Zeng, Y., Pelgrum, H., Wonink, S., & Karimi, P. (2020). Evaluation of WaPOR V2 evapotranspiration products across Africa. *Hydrological Processes*, *34*, 3200–3221. https://doi.org/10.1002/hyp.13791

Bonsor, H. C., MacDonald, A. M., & Davies, J. (2014). Evidence for extreme variations in the permeability of laterite from a detailed analysis of well behaviour in Nigeria. *Hydrological Processes*, *28*, 3563–3573. https://doi.org/10.1002/hyp.9871

Brocca, L., Ciabatta, L., Massari, C., Camici, S., & Tarpanelli, A. (2017). Soil moisture for hydrological applications: Open questions and new opportunities. *Water*, *9*, 140. https://doi.org/10.3390/w9020140

Budyko, M. I. (1961). The heat balance of the Earth's surface. *Soviet Geography*, *2*, 3–13. https://doi.org/10.1080/00385417.1961.10770761

Cecil, D. J., Buechler, D. E., & Blakeslee, R. J. (2014). Gridded lightning climatology from TRMM-LIS and OTD: Dataset description. *Atmospheric Research*, *135–136*, 404–414. https://doi.org/10.1016/j.atmosres.2012.06.028

Cleugh, H. A., Leuning, R., Mu, Q., & Running, S. W. (2007). Regional evaporation estimates from flux tower and MODIS satellite data. *Remote Sensing of Environment*, *106*, 285–304. https://doi.org/10.1016/j.rse.2006.07.007

Coz, C. L., & van de Giesen, N. (2020). Comparison of rainfall products over sub-Saharan Africa. *Journal of Hydrometeorology*, *21*, 553–596. https://doi.org/10.1175/JHM-D-18-0256.1

Cuthbert, M. O., Taylor, R. G., Favreau, G., Todd, M. C., Shamsudduha, M., Villholth, K. G., MacDonald, A. M., Scanlon, B. R., Kotchoni, D. O. V., Vouillamoz, J.-M., Lawson, F. M. A., Adjomayi, P. A., Kashaigili, J., Seddon, D., Sorensen, J. P. R., Ebrahim, G. Y., Owor, M., Nyenje, P. M., Nazoumou, Y., et al. (2019). Observed controls on resilience of groundwater to climate variability in sub-Saharan Africa. *Nature*, *572*, 230–234. https://doi.org/10.1038/s41586-019-1441-7

Dai, Y., Xin, Q., Wei, N., Zhang, Y., Shangguan, W., Yuan, H., Zhang, S., Liu, S., & Lu, X. (2019). A global high-resolution data set of soil hydraulic and thermal properties for land surface modeling. *Journal of Advances in Modeling Earth Systems*, *11*, 2996–3023. https://doi.org/10.1029/2019MS001784

Daly, C., Neilson, R. P., & Phillips, D. L. (1994). A statistical-topographic model for mapping climatological precipitation over mountainous terrain. *Journal of Applied Meteorology and Climatology*, *33*, 140–158. https://doi.org/10.1175/1520-0450(1994)033<0140:ASTMFM>2.0.CO;2

Dembélé, M., Schaefli, B., van de Giesen, N., & Mariéthoz, G. (2020). Suitability of 17 rainfall and temperature gridded datasets for largescale-hydrological modelling in West Africa. *Hydrology and Earth System Sciences*, *24*, 5379–5406. https://doi.org/10.5194/hess-2020-68

Dezfuli, A. K., Ichoku, C. M., Huffman, G. J., Mohr, K. I., Selker, J. S., van de Giesen, N., Hochreutener, R., & Annor, F. O. (2017). Validation of IMERG precipitation in Africa. *Journal of Hydrometeorology*, *18*, 2817–2825. https://doi.org/10.1175/JHM-D-17-0139.1

Dinku, T., Funk, C., Peterson, P., Maidment, R., Tadesse, T., Gadain, H., & Ceccato, P. (2018). Validation of the CHIRPS satellite rainfall estimates over eastern Africa. *Quarterly Journal of the Royal Meteorological Society*, *144*, 292–312. https://doi.org/10.1002/qj.3244

Dorigo, W., Wagner, W., Albergel, C., Albrecht, F., Balsamo, G., Brocca, L., Chung, D., Ertl, M., Forkel, M., Gruber, A., Haas, E., Hamer, P. D., Hirschi, M., Ikonen, J., de Jeu, R., Kidd, R., Lahoz, W., Liu, Y. Y., Miralles, D., et al. (2017). ESA CCI soil moisture for improved earth system understanding: State-of-the art and future directions. *Remote Sensing of Environment*, *203*, 185–215. https://doi.org/10.1016/j.rse.2017.07.001

Fan, Y., Li, H., & Miguez-Macho, G. (2013). Global patterns of groundwater table depth. *Science*, *339*, 940–943. https://doi.org/10.1126/science.1229881

Franz, T. E., Caylor, K. K., King, E. G., Nordbotten, J. M., Celia, M. A., & Rodríguez-Iturbe, I. (2012). An ecohydrological approach to predicting hillslope-scale vegetation patterns in dryland ecosystems. *Water Resources Research*, *48*, W01515. https://doi.org/10.1029/2011WR010524

Franz, T. E., Caylor, K. K., Nordbotten, J. M., Rodríguez-Iturbe, I., & Celia, M. A. (2010). An ecohydrological approach to predicting regional woody species distribution patterns in dryland ecosystems. *Advances in Water Resources*, *33*, 215–230. https://doi.org/10.1016/j.advwatres.2009.12.003

Fu, S., Sonnenborg, T. O., Jensen, K. H., & He, X. (2011). Impact of precipitation spatial resolution on the hydrological response of an integrated distributed water resources model. *Vadose Zone Journal*, *10*, 25–36. https://doi.org/10.2136/vzj2009.0186

Gichuki, F. N. (2002). Water scarcity and conflicts: A casestudy of the Upper Ewaso Ng'iro North Basin. In Blank, H.G., Mutero, C.M., Murray-Rust, H., editors. *The changing face of irrigation in Kenya: Opportunitiesfor anticipating change in eastern and southern Africa (pp. 113–134)*. International Water Management Institute.

Gichuki, F. N. (2004). Managing the externalities of declining dry season river flow: A case study from the Ewaso Ngiro North River basin, Kenya. *Water Resources Research*, *40*, W08S03. https://doi.org/10.1029/2004WR003106

Gleeson, T., Moosdorf, N., Hartmann, J., & van Beek, L. P. H. (2014). A glimpse beneath earth's surface: GLobal HYdrogeology MaPS (GLHYMPS) of permeability and porosity. *Geophysical Research Letters*, *41*, 3891–3898. https://doi.org/10.1002/2014GL059856

Goodrich, D. C., Faurès, J.-M., Woolhiser, D. A., Lane, L. J., & Sorooshian, S. (1995). Measurement and analysis of small-scale convective storm rainfall variability. *Journal of Hydrology*, *173*, 283–308. https://doi.org/10.1016/0022-1694(95)02703-R

Goodrich, D. C., Kepner, W. G., Levick, L. R., & Wigington, P. J. (2018). Southwestern intermittent and ephemeral stream connectivity. *JAWRA Journal of the American Water Resources Association*, *54*, 400–422. https://doi.org/10.1111/1752-1688.12636

Goodrich, D. C., Lane, L. J., Shillito, R. M., Miller, S. N., Syed, K. H., & Woolhiser, D. A. (1997). Linearity of basin response as a function of scale in a semiarid watershed. *Water Resources Research*, *33*, 2951–2965. https://doi.org/10.1029/97WR01422

Goodrich, D. C., Williams, D. G., Unkrich, C. L., Hogan, J. F., Scott, R. L., Hultine, K. R., Pool, D., Goes, A. L., & Miller, S. (2013). Comparison of methods to estimate Ephemeral Channel recharge, walnut gulch, San Pedro River basin, Arizona. In *Groundwater recharge in a desert environment: The southwestern United States* (pp. 77–99). American Geophysical Union (AGU).

Groisman, P. Y., & Legates, D. R. (1994). The accuracy of United States precipitation data. *Bulletin of the American Meteorological Society*, *75*,

215–228. https://doi.org/10.1175/1520-0477(1994)075<0215:TAOUSP>2.0.CO;2

Gudmundsson, L., Greve, P., & Seneviratne, S. I. (2016). The sensitivity of water availability to changes in the aridity index and other factors—A probabilistic analysis in the Budyko space. *Geophysical Research Letters*, *43*, 6985–6994. https://doi.org/10.1002/2016GL069763

Guilloteau, C., Roca, R., & Gosset, M. (2016). A multiscale evaluation of the detection capabilities of high-resolution satellite precipitation products in West Africa. *Journal of Hydrometeorology*, *17*, 2041–2059. https://doi.org/10.1175/JHM-D-15-0148.1

Gupta, H. V., Kling, H., Yilmaz, K. K., & Martinez, G. F. (2009). Decomposition of the mean squared error and NSE performance criteria: Implications for improving hydrological modelling. *Journal of Hydrology*, *377*, 80–91. https://doi.org/10.1016/j.jhydrol.2009.08.003

Henn, B., Newman, A. J., Livneh, B., Daly, C., & Lundquist, J. D. (2018). An assessment of differences in gridded precipitation datasets in complex terrain. *Journal of Hydrology*, *556*, 1205–1219. https://doi.org/10.1016/j.jhydrol.2017.03.008

Hersbach, H., Bell, B., Berrisford, P., Hirahara, S., Horányi, A., Muñoz-Sabater, J., Nicolas, J., Peubey, C., Radu, R., Schepers, D., Simmons, A., Soci, C., Abdalla, S., Abellan, X., Balsamo, G., Bechtold, P., Biavati, G., Bidlot, J., Bonavita, M., et al. (2020). The ERA5 global reanalysis. *Quarterly Journal of the Royal Meteorological Society*, *146*, 1999–2049. https://doi.org/10.1002/qj.3803

Huang, J., Li, Y., Fu, C., Chen, F., Fu, Q., Dai, A., Shinoda, M., Ma, Z., Guo, W., Li, Z., Zhang, L., Liu, Y., Yu, H., He, Y., Xie, Y., Guan, X., Ji, M., Lin, L., Wang, S., et al. (2017). Dryland climate change: Recent progress and challenges. *Reviews of Geophysics*, *55*, 719–778. https://doi.org/10.1002/2016RG000550

Huang, Y., Bárdossy, A., & Zhang, K. (2019). Sensitivity of hydrological models to temporal and spatial resolutions of rainfall data. *Hydrology and Earth System Sciences*, *23*, 2647–2663. https://doi.org/10.5194/hess-23-2647-2019

Huffman, G. J., Bolvin, D. T., Braithwaite, D., Hsu, K., Joyce, R., Xie, P., & Yoo, S.-H. (2015). Algorithm Theoretical Basis Document (ATBD) Version. In *NASA global precipitation measurement (GPM) integrated multi-satellite retrievals for GPM (IMERG)* (Vol. 4, p. 26). NASA.

IPCC6. (2021). *Climate change 2021: The physical science basis. Contribution of working group I to the sixth assessment report of the intergovernmental panel on climate change*. Cambridge University Press.

Jahangir, M. H., & Arast, M. (2020). Remote sensing products for predicting actual evapotranspiration and water stress footprints under different land cover. *Journal of Cleaner Production*, *266*, 121818. https://doi.org/10.1016/j.jclepro.2020.121818

Jiao, D., Xu, N., Yang, F., & Xu, K. (2021). Evaluation of spatial-temporal variation performance of ERA5 precipitation data in China. *Scientific Reports*, *11*, 17956. https://doi.org/10.1038/s41598-021-97432-y

Kiptala, J. K., Mohamed, Y., Mul, M. L., & Van der Zaag, P. (2013). Mapping evapotranspiration trends using MODIS and SEBAL model in a data scarce and heterogeneous landscape in eastern Africa. *Water Resources Research*, *49*, 8495–8510. https://doi.org/10.1002/2013WR014240

Knoben, W. J. M., Freer, J. E., & Woods, R. A. (2019). Technical note: Inherent benchmark or not? Comparing Nash–Sutcliffe and Kling–Gupta efficiency scores. *Hydrology and Earth System Sciences*, *23*, 4323–4331. https://doi.org/10.5194/hess-23-4323-2019

Krause, P., Boyle, D. P., & Bäse, F. (2005). Comparison of different efficiency criteria for hydrological model assessment. *Advances in Geosciences*, *5*, 89–97.

Landerer, F. W., & Swenson, S. C. (2012). Accuracy of scaled GRACE terrestrial water storage estimates. *Water Resources Research*, *48*, W04531. https://doi.org/10.1029/2011WR011453

Leenaars, J. G. B., Claessens, L., Heuvelink, G. B. M., Hengl, T., Ruiperez González, M., van Bussel, L. G. J., Guilpart, N., Yang, H., & Cassman, K. G. (2018). Mapping rootable depth and root zone plant-available water holding capacity of the soil of sub-Saharan Africa. *Geoderma*, *324*, 18–36. https://doi.org/10.1016/j.geoderma.2018.02.046

Lettenmaier, D. P., Alsdorf, D., Dozier, J., Huffman, G. J., Pan, M., & Wood, E. F. (2015). Inroads of remote sensing into hydrologic science during the WRR era. *Water Resources Research*, *51*, 7309–7342. https://doi.org/10.1002/2015WR017616

Li, L., Ngongondo, C. S., Xu, C.-Y., & Gong, L. (2012). Comparison of the global TRMM and WFD precipitation datasets in driving a large-scale hydrological model in southern Africa. *Hydrology Research*, *44*, 770–788. https://doi.org/10.2166/nh.2012.175

Liniger, H., Gikonyo, J., Kiteme, B., & Wiesmann, U. (2005). Assessing and managing scarce Tropical Mountain water resources. *Mountain Research and Development*, *25*, 163–173. https://doi.org/10.1659/0276-4741(2005)025[0163:AAMSTM]2.0.CO;2

Liu, Y. Y., Parinussa, R. M., Dorigo, W. A., De Jeu, R. A. M., Wagner, W., van Dijk, A. I. J. M., McCabe, M. F., & Evans, J. P. (2011). Developing an improved soil moisture dataset by blending passive and active microwave satellite-based retrievals. *Hydrology and Earth System Sciences*, *15*, 425–436. https://doi.org/10.5194/hess-15-425-2011

Longuevergne, L., Scanlon, B. R., & Wilson, C. R. (2010). GRACE hydrological estimates for small basins: Evaluating processing approaches on the High Plains aquifer, USA. *Water Resources Research*, *46*(11), W11517. https://doi.org/10.1029/2009WR008564

Lundquist, J. D., Hughes, M., Henn, B., Gutmann, E. D., Livneh, B., Dozier, J., & Neiman, P. (2015). High-elevation precipitation patterns: Using snow measurements to assess daily gridded datasets across the Sierra Nevada, California. *Journal of Hydrometeorology*, *16*, 1773–1792. https://doi.org/10.1175/JHM-D-15-0019.1

Ly, S., Charles, C., & Degré, A. (2013). Different methods for spatial interpolation of rainfall data for operational hydrology and hydrological modeling at watershed scale: A review. *Biotechnology, Agronomy and Society and Environment*, *17*(2), 392-406.

MacDonald, A. M., Lark, R. M., Taylor, R. G., Abiye, T., Fallas, H. C., Favreau, G., Goni, I. B., Kebede, S., Scanlon, B., Sorensen, J. P. R., Tijani, M., Upton, K. A., & West, C. (2021). Mapping groundwater recharge in Africa from ground observations and implications for water security. *Environmental Research Letters*, *16*, 034012. https://doi.org/10.1088/1748-9326/abd661

Macharia, J. M., Ngetich, F. K., & Shisanya, C. A. (2020). Comparison of satellite remote sensing derived precipitation estimates and observed data in Kenya. *Agricultural and Forest Meteorology*, *284*, 107875. https://doi.org/10.1016/j.agrformet.2019.107875

Maggioni, V., Meyers, P. C., & Robinson, M. D. (2016). A review of merged high-resolution satellite precipitation product accuracy during the tropical rainfall measuring Mission (TRMM) era. *Journal of Hydrometeorology*, *17*, 1101–1117. https://doi.org/10.1175/JHM-D-15-0190.1

Massari, C., Crow, W., & Brocca, L. (2017). An assessment of the performance of global rainfall estimates without ground-based observations. *Hydrology and Earth System Sciences*, *21*, 4347–4361. https://doi.org/10.5194/hess-21-4347-2017

Mati, B. M., Muchiri, J. M., Njenga, K., de Vries, F. P., & Merrey, D. J. (2006). *Assessing water availability under pastoral livestock systems in drought-prone Isiolo District*. IWMI.

Mayes, M., Caylor, K. K., Singer, M. B., Stella, J. C., Roberts, D., & Nagler, P. (2020). Climate sensitivity of water use by riparian woodlands at landscape scales. *Hydrological Processes*, *34*, 4884–4903. https://doi.org/10.1002/hyp.13942

McMillan, H., Krueger, T., & Freer, J. (2012). Benchmarking observational uncertainties for hydrology: Rainfall, river discharge and water quality. *Hydrological Processes*, *26*, 4078–4111. https://doi.org/10.1002/hyp.9384

Miralles, D. G., Jiménez, C., Jung, M., Michel, D., Ershadi, A., McCabe, M. F., Hirschi, M., Martens, B., Dolman, A. J., Fisher, J. B., Mu, Q., Seneviratne, S. I., Wood, E. F., & Fernández-Prieto, D. (2016). The WACMOS-ET project – part 2: Evaluation of global terrestrial

evaporation data sets. *Hydrology and Earth System Sciences*, *20*, 823–842. https://doi.org/10.5194/hess-20-823-2016

Mu, Q., Heinsch, F. A., Zhao, M., & Running, S. W. (2007). Development of a global evapotranspiration algorithm based on MODIS and global meteorology data. *Remote Sensing of Environment*, *111*, 519–536. https://doi.org/10.1016/j.rse.2007.04.015

Muriithi, F. K. (2016). Land use and land cover (LULC) changes in semi-arid sub-watersheds of Laikipia and Athi River basins, Kenya, as influenced by expanding intensive commercial horticulture. *Remote Sensing Applications: Society and Environment*, *3*, 73–88. https://doi.org/10.1016/j.rsase.2016.01.002

Mutiga, J. K., Mavengano, S. T., Zhongbo, S., Woldai, T., & Becht, R. (2010). Water allocation as a planning tool to minimise water use conflicts in the upper Ewaso Ng'iro North Basin, Kenya. *Water Resources Management*, *24*, 3939–3959. https://doi.org/10.1007/s11269-010-9641-9

Ngigi, S. N., Savenije, H. H. G., & Gichuki, F. N. (2007). Land use changes and hydrological impacts related to up-scaling of rainwater harvesting and management in upper Ewaso Ng'iro river basin, Kenya. *Land Use Policy*, *24*, 129–140. https://doi.org/10.1016/j.landusepol.2005.10.002

Ngigi, S. N., Savenije, H. H. G., & Gichuki, F. N. (2008). Hydrological impacts of flood storage and management on irrigation water abstraction in upper Ewaso Ng'iro River Basin, Kenya. *Water Resources Management*, *22*, 1859–1879. https://doi.org/10.1007/s11269-008-9257-5

Notter, B., MacMillan, L., Viviroli, D., Weingartner, R., & Liniger, H.-P. (2007). Impacts of environmental change on water resources in the Mt. Kenya region. *Journal of Hydrology*, *343*, 266–278. https://doi.org/10.1016/j.jhydrol.2007.06.022

Obled, C., Wendling, J., & Beven, K. (1994). The sensitivity of hydrological models to spatial rainfall patterns: An evaluation using observed data. *Journal of Hydrology*, *159*, 305–333. https://doi.org/10.1016/0022-1694(94)90263-1

Padrón, R. S., Gudmundsson, L., Greve, P., & Seneviratne, S. I. (2017). Large-scale controls of the surface water balance over land: Insights from a systematic review and meta-analysis. *Water Resources Research*, *53*, 9659–9678. https://doi.org/10.1002/2017WR021215

Pelletier, J. D., Broxton, P. D., Hazenberg, P., Zeng, X., Troch, P. A., Niu, G.-Y., Williams, Z., Brunke, M. A., & Gochis, D. (2016). A gridded global data set of soil, intact regolith, and sedimentary deposit thicknesses for regional and global land surface modeling. *Journal of Advances in Modeling Earth Systems*, *8*, 41–65. https://doi.org/10.1002/2015MS000526

Pilgrim, D. H., Chapman, T. G., & Doran, D. G. (1988). Problems of rainfall-runoff modelling in arid and semiarid regions. *Hydrological Sciences Journal*, *33*, 379–400. https://doi.org/10.1080/02626668809491261

Pollock, M. D., O'Donnell, G., Quinn, P., Dutton, M., Black, A., Wilkinson, M. E., Colli, M., Stagnaro, M., Lanza, L. G., Lewis, E., Kilsby, C. G., & O'Connell, P. E. (2018). Quantifying and mitigating wind-induced Undercatch in rainfall measurements. *Water Resources Research*, *54*, 3863–3875. https://doi.org/10.1029/2017WR022421

Preimesberger, W., Scanlon, T., Su, C.-H., Gruber, A., & Dorigo, W. (2021). Homogenization of structural breaks in the global ESA CCI soil moisture multisatellite climate data record. *IEEE Transactions on Geoscience and Remote Sensing*, *59*, 2845–2862. https://doi.org/10.1109/TGRS.2020.3012896

Quichimbo, E. A. (2016). *Understanding the sensitivity of focused, indirect groundwater recharge to climate change (MSc)*. University of Birmingham.

Quichimbo, E. A. (2021). *Modelling water partitioning in dryland regions: A multiscale analysis*. Cardiff University.

Quichimbo, E. A., Singer, M. B., & Cuthbert, M. O. (2020). Characterising groundwater–surface water interactions in idealised ephemeral stream systems. *Hydrological Processes*, *34*, 3792–3806. https://doi.org/10.1002/hyp.13847

Quichimbo, E. A., Singer, M. B., Michaelides, K., Hobley, D. E. J., Rosolem, R., & Cuthbert, M. O. (2021). DRYP 1.0: A parsimonious hydrological model of DRYland partitioning of the water balance. *Geoscientific Model Development*, *14*, 6893–6917. https://doi.org/10.5194/gmd-14-6893-2021

Rios Gaona, M. F., Michaelides, K., & Singer, M. B. (2023). STORM v.2: A simple, stochastic decision-support tool for exploring the impacts of climate and climate change at, and near the land surface in gauged watersheds. *Geoscientific Model Development Discussion*, *1–36*. https://doi.org/10.5194/gmd-2023-98

Rowlands, D. D., Luthcke, S. B., Klosko, S. M., Lemoine, F. G. R., Chinn, D. S., McCarthy, J. J., Cox, C. M., & Anderson, O. B. (2005). Resolving mass flux at high spatial and temporal resolution using GRACE intersatellite measurements. *Geophysical Research Letters*, *32*, L04310. https://doi.org/10.1029/2004GL021908

Running, S., Qiaozhen, M., & Maosheng, Z. (2017). *MOD16A2 MODIS/Terra net evapotranspiration 8-day L4 global 500m SIN grid V006*. LAADS DAAC. https://doi.org/10.5067/MODIS/MOD16A2.006

Satgé, F., Hussain, Y., Molina-Carpio, J., Pillco, R., Laugner, C., Akhter, G., & Bonnet, M.-P. (2021). Reliability of SM2RAIN precipitation datasets in comparison to gauge observations and hydrological modelling over arid regions. *International Journal of Climatology*, *41*, E517–E536. https://doi.org/10.1002/joc.6704

Save, H., Bettadpur, S., & Tapley, B. D. (2016). High-resolution CSR GRACE RL05 mascons. *Journal of Geophysical Research – Solid Earth*, *121*, 7547–7569. https://doi.org/10.1002/2016JB013007

Scanlon, B. R., Faunt, C. C., Longuevergne, L., Reedy, R. C., Alley, W. M., McGuire, V. L., & McMahon, P. B. (2012). Groundwater depletion and sustainability of irrigation in the US High Plains and Central Valley. *Proceedings of the National Academy of Sciences*, *109*, 9320–9325. https://doi.org/10.1073/pnas.1200311109

Schreiner-McGraw, A., Ajami, H., & Vivoni, E. R. (2019). Extreme weather events and transmission losses in arid streams. *Environmental Research Letters*, *14*, 084002. https://doi.org/10.1088/1748-9326/ab2949

Schreiner-McGraw, A. P., & Ajami, H. (2020). Impact of uncertainty in precipitation forcing data sets on the hydrologic budget of an integrated hydrologic model in mountainous terrain. *Water Resources Research*, *56*, e2020WR027639. https://doi.org/10.1029/2020WR027639

Scoging, H. M., & Thornes, J. B. (1979). *Infiltration characteristics in a semi-arid environment, in: The hydrology of areas of low precipitation* (pp. 159–168). IAHS Publication.

Shanafield, M., & Cook, P. G. (2014). Transmission losses, infiltration and groundwater recharge through ephemeral and intermittent streambeds: A review of applied methods. *Journal of Hydrology*, *511*, 518–529. https://doi.org/10.1016/j.jhydrol.2014.01.068

Singer, M. B., Asfaw, D. T., Rosolem, R., Cuthbert, M. O., Miralles, D. G., MacLeod, D., Quichimbo, E. A., & Michaelides, K. (2021). Hourly potential evapotranspiration at 0.1° resolution for the global land surface from 1981-present. *Scientific Data*, *8*, 224. https://doi.org/10.1038/s41597-021-01003-9

Singer, M. B., Michaelides, K., & Hobley, D. E. J. (2018). STORM 1.0: A simple, flexible, and parsimonious stochastic rainfall generator for simulating climate and climate change. *Geoscientific Model Development*, *11*, 3713–3726. https://doi.org/10.5194/gmd-11-3713-2018

Stisen, S., & Sandholt, I. (2010). Evaluation of remote-sensing-based rainfall products through predictive capability in hydrological runoff modelling. *Hydrological Processes*, *24*, 879–891. https://doi.org/10.1002/hyp.7529

Su, F., Hong, Y., & Lettenmaier, D. P. (2008). Evaluation of TRMM multisatellite precipitation analysis (TMPA) and its utility in hydrologic prediction in the La Plata Basin. *Journal of Hydrometeorology*, *9*, 622–640.

Sylla, M. B., Giorgi, F., Coppola, E., & Mariotti, L. (2013). Uncertainties in daily rainfall over Africa: Assessment of gridded observation products and evaluation of a regional climate model simulation. *International Journal of Climatology*, *33*, 1805–1817. https://doi.org/10.1002/joc.3551

Tang, G., Clark, M. P., Papalexiou, S. M., Ma, Z., & Hong, Y. (2020). Have satellite precipitation products improved over last two decades? A comprehensive comparison of GPM IMERG with nine satellite and reanalysis datasets. *Remote Sensing of Environment*, *240*, 111697. https://doi.org/10.1016/j.rse.2020.111697

Tang, G., Zeng, Z., Long, D., Guo, X., Yong, B., Zhang, W., & Hong, Y. (2016). Statistical and hydrological comparisons between TRMM and GPM Level-3 products over a Midlatitude Basin: Is Day-1 IMERG a good successor for TMPA 3B42V7? *Journal of Hydrometeorology*, *17*, 121–137. https://doi.org/10.1175/JHM-D-15-0059.1

Thornton, P. E., Running, S. W., & White, M. A. (1997). Generating surfaces of daily meteorological variables over large regions of complex terrain. *Journal of Hydrology*, *190*, 214–251. https://doi.org/10.1016/S0022-1694(96)03128-9

Trambauer, P., Dutra, E., Maskey, S., Werner, M., Pappenberger, F., van Beek, L. P. H., & Uhlenbrook, S. (2014). Comparison of different evaporation estimates over the African continent. *Hydrology and Earth System Sciences*, *18*, 193–212. https://doi.org/10.5194/hess-18-193-2014

UNEP. (1992). *World atlas of desertification. United Nations environment Programme* (2nd ed.). Edward Arnold.

Velpuri, N. M., Senay, G. B., Singh, R. K., Bohms, S., & Verdin, J. P. (2013). A comprehensive evaluation of two MODIS evapotranspiration products over the conterminous United States: Using point and gridded FLUXNET and water balance ET. *Remote Sensing of Environment*, *139*, 35–49. https://doi.org/10.1016/j.rse.2013.07.013

Watkins, M. M., Wiese, D. N., Yuan, D.-N., Boening, C., & Landerer, F. W. (2015). Improved methods for observing Earth's time variable mass distribution with GRACE using spherical cap mascons. *Journal of Geophysical Research – Solid Earth*, *120*, 2648–2671. https://doi.org/10.1002/2014JB011547

Weerasinghe, I., Bastiaanssen, W., Mul, M., Jia, L., & van Griensven, A. (2020). Can we trust remote sensing evapotranspiration products over Africa? *Hydrology and Earth System Sciences*, *24*, 1565–1586. https://doi.org/10.5194/hess-24-1565-2020

Westrick, K. J., Mass, C. F., & Colle, B. A. (1999). The limitations of the WSR-88D radar network for quantitative precipitation measurement over the coastal Western United States. *Bulletin of the American Meteorological Society*, *80*, 2289–2298. https://doi.org/10.1175/1520-0477(1999)080<2289:TLOTWR>2.0.CO;2

Wheater, H., Sorooshian, S., & Sharma, I. K. D. (2008). *Hydrological modelling in arid and semi-arid areas*. Cambridge University Press.

Wheater, H., Sorooshian, S., & Sharma, K. D. (2007). *Hydrological modelling in arid and semi-arid areas* (1st ed.). Cambridge University Press.

WRAP. (1987). *Water resources assessment study in Laikipia, water resources assessment program (WRAP)*. Ministry of Water Development Report.

Zhu, Z., Wright, D. B., & Yu, G. (2018). The impact of rainfall space-time structure in flood frequency analysis. *Water Resources Research*, *54*, 8983–8998. https://doi.org/10.1029/2018WR023550

Zoccatelli, D., Marra, F., Smith, J., Goodrich, D., Unkrich, C., Rosensaft, M., & Morin, E. (2020). Hydrological modelling in desert areas of the eastern Mediterranean. *Journal of Hydrology*, *587*, 124879. https://doi.org/10.1016/j.jhydrol.2020.124879

SUPPORTING INFORMATION

Additional supporting information can be found online in the Supporting Information section at the end of this article.

How to cite this article: Quichimbo, E. A., Singer, M. B., Michaelides, K., Rosolem, R., MacLeod, D. A., Asfaw, D. T., & Cuthbert, M. O. (2023). Assessing the sensitivity of modelled water partitioning to global precipitation datasets in a data-scarce dryland region. *Hydrological Processes*, *37*(12), e15047. https://doi.org/10.1002/hyp.15047